Bifurcations of n-homoclinic orbits in optically injected lasers

Sebastian Wieczorek

Sandia National Laboratories, P.O. Box 5800, Ms 0601, Albuquerque, NM 87185 – 0601, USA

Bernd Krauskopf

Department of Engineering Mathematics, University of Bristol, BS8 1TR, U.K.

Abstract.

We study in detail complex structures of homoclinic bifurcations in a three-dimensional rate-equation model of a semiconductor laser receiving optically injected light of amplitude K and frequency detuning ω. Specifically, we find and follow in the (K, ω)-plane curves of n-homoclinic bifurcations, where a saddle-focus is connected to itself at the n-th return to a neighborhood of the saddle. We reveal an intricate interplay of codimension-two double-homoclinic and T-point bifurcations. Furthermore, we study how the bifurcation diagram changes with an additional parameter, the so-called linewidth enhancement factor α of the laser. In particular, we find folds (minima) of T-point bifurcation and double-homoclinic bifurcation curves, which are accumulated by infinitely many changes of the bifurcation diagram due to transitions through singularities of surfaces of homoclinic bifurcations.

The injection laser emerges as a system that allows one to study codimension-two bifurcations of n-homoclinic orbits in a concrete vector field. At the same time, the bifurcation diagram in the (K, ω)-plane is of physical relevance. An example is the identification of regions, and their dependence on the parameter α, of multi-pulse excitability where the laser reacts to a single small perturbation by sending out n pulses.

Submitted to: *Nonlinearity*

AMS classification scheme numbers: 34C37, 70K44, 37Gxx, 37N20

1. Introduction

We present a detailed study of homoclinic orbits to a saddle-focus (a saddle point with one real and a pair of complex conjugate eigenvalues) [1, 2, 3, 4] and their bifurcations in a three-dimensional vector field model of an *optically injected laser*. Such a laser receives optically injected light of a given fixed amplitude K and frequency ω; the laser is specified by a number of material constants, so that the model is valid for solid-state, $C0_2$ and semiconductor lasers; see section 2 for details.

The work presented here is similar in spirit to the study of other three-dimensional dynamical systems arising in applications that feature saddle-focus homoclinic orbits, for example, the models of chemical reactions in Refs. [5, 6], the model for calcium waves in cells Ref. [7], and the simplified weather model Ref. [8]. The direct motivation was the discovery of the new physical effect of multi-pulse excitability in the injection laser [9]: as the result of a single perturbation the laser may react by sending out an n-pulse response. This phenomenon occurs near an n-homoclinic orbit, which closes up only at the n-th return to a small neighborhood of the saddle-focus. It turns out that the associated curves of n-homoclinic bifurcations in the (K, ω)-plane are arranged in an intricate structure inside regions that are bounded by 1-homoclinic bifurcations and which we call *homoclinic teeth*.

In this paper we study these intricate structures of n-homoclinic orbits and their bifurcations in considerable detail. The rate equation model of an injection laser is a concrete dynamical system in which such global bifurcations can be found and studied with numerical tools, in particular, the continuation of periodic and connecting orbits. This reveals how codimension-two homoclinic bifurcations act as organizing centers of the bifurcation diagram. First, we find heteroclinic cycles known as T-point bifurcations; we are dealing here with the case that both saddles involved have a pair of complex conjugate eigenvalues. Such T-point bifurcations were found in systems from applications [7, 10, 11, 12, 13, 14, 15, 16] and their unfolding is known to involve n-homoclinic orbits for any n [17, 18]. Secondly, we find double-homoclinic orbits to a saddle-focus, where there are two different homoclinic connections to a single saddle-focus. (This should not be confused with a 2-homoclinic orbit.) This codimension-two global bifurcation has been studied in an abstract setting in Refs. [19, 20, 21]. The bifurcations of 1-homoclinic orbits are known, but the possible unfoldings are not yet fully understood. We present sketches of relevant bifurcation curves associated with these global bifurcations and show with numerical bifurcation diagrams how they manifest themselves in the optically injected laser model.

Finally, we show that curves of codimension-two global bifurcations may have folds, in our case minima with respect to the physically relevant linewidth enhancement factor; see section 2. We show how such a minimum is accumulated by singularity transitions through saddles and extrema of associated codimension-one surfaces of homoclinic bifurcations.

This paper is organized as follows. In section 2 we introduce the rate equation model for an optically injected laser and present some background information on the system. In section 3 we introduce the homoclinic teeth in the locking region in the (K, ω)-plane, and show how they grow with the linewidth-enhancement factor α. Section 4 then considers the complex structure of n-homoclinic orbits inside the homoclinic teeth and explains how this gives rise to multi-pulse excitability. We then discuss in section 5 codimension-two bifurcations of homoclinic and heteroclinic orbits and show how they organize the overall dynamics. Section 6 is a phenomenological description of codimension-three phenomena that one encounters when α is changed.

Finally, in section 7 we draw some conclusions and point to future work.

All curves of global bifurcations and the associated homoclinic and heteroclinic orbits were calculated with the HomCont [22, 23] part of the continuation package AUTO [24]; the invariant manifolds and time series illustrating multi-pulse excitability were computed with the package DsTool [25].

2. The optically injected laser

From the physical perspective, a semiconductor laser with optical injection is one of the 'oldest' laser systems that has been studied; see the review papers Refs. [26, 27] and Ref. [28] as general references to the extensive literature. Because the first types of (semiconductor) lasers had a very wide linewidth (frequency distribution) and other instabilities, the idea was to improve their characteristics by subjecting them to a small amount of 'clean' light from a second laser. In this way, it is possible to get the laser to lase at the frequency of the injected light and with a much reduced linewidth [29, 30, 31].

From the dynamical systems point of view, a class-B laser (the active-medium polarization decays much faster than the population inversion and the electric field) with optical injection as discussed here is one of the nicest physical systems to show a fascinating array of nonlinear dynamics. Several kinds of complex and chaotic dynamics were discovered; see, for example, Refs. [32, 33, 34, 35, 36, 37]. Of particular importance is the fact that this system is very well described by a set of three autonomous ordinary differential equations for the complex electric field $E = E_x + iE_y$ and the population inversion n (the number of electron-hole pairs in case of a semiconductor laser) [28, 38]. These so-called *single-mode rate equations* can be written in dimensionless form as

$$\begin{aligned} \dot{E} &= K + \left(\frac{1}{2}(1+i\alpha)n - i\omega\right) E \\ \dot{n} &= -2\Gamma n - (1+2Bn)(|E|^2 - 1) \ . \end{aligned} \tag{1}$$

The two main parameters are the injected field amplitude K and the detuning ω, the frequency difference between the injected light and the frequency of the laser without injection. While K and ω can easily be changed in an experiment, the parameters B, Γ and α describe material properties of a given laser. Specifically, B is the rescaled life time of photons in the laser cavity and Γ is the rescaled damping rate of the so-called relaxation oscillations, an exchange of energy between the electric field E and the population n of a typical frequency of around few GHz. We use the realistic values $B = 0.015$ and $\Gamma = 0.035$ throughout in our study.

While B and Γ are known not to influence the dynamics of the injected laser very much [39], the material constant α, called the *linewidth enhancement factor*, can be very different for different lasers, and it is known that changing α has a very large effect [28]. The parameter α describes the coupling between the phase and the amplitude of the electric field E, and it is in the range of $\alpha \in [1, 10]$ for typical semiconductor lasers. On the other hand, Eq. (1) for $\alpha = 0$ models injected solid-state and CO_2 lasers, which have a negligible phase-amplitude coupling. This is our motivation for studying how the

bifurcation set in the (K, ω)-plane depends on α, that is, on the main material property of the particular laser under consideration.

We now briefly summarize some previous work on the dynamics and bifurcations of injection lasers. The rate equations (1) have been studied (in equivalent forms of rescaling) by numerical simulation (see, for example, [35, 37, 39, 40]) and the derivation of reduced equations by considering certain limits [41, 42, 43, 44]. However, their study with tools from bifurcation theory arguably started with the work of Solari and Oppo in Ref. [45], who derived and analyzed a reduction to a two-dimensional vector field near a codimension-two saddle-node Hopf (SNH) point. This work was followed up in Ref. [46] by considering the global dynamics near the SNH point in the full three-dimensional rate equations. In a similar vein, a two-dimensional vector field approximation of the injection laser was derived in Ref. [47], and then studied in Ref. [48] with normal form theory near the SNH point. Predicted stable and unstable tori were then indeed found in the full rate equations in Ref. [49], which were then derived in the dimensionless form (1) in Ref. [28]. Quite a number of studies now exist that show the amazing complexity of bifurcations in the full rate equations, including different types of multistability = [37, 50, 51] and routes to chaos [52, 53], unnested islands of period-doublings [54], and complex bifurcation structures associated with the route to locking [55, 56, 57, 58]. As was already mentioned, the motivation for this paper was the discovery of multipulse excitability in the injection laser in Ref. [9]; see also Ref. [59] and section 4.

Equation (1) describes a laser that lases at a single laser mode throughout. This is ensured for so-called distributed feedback (DFB) lasers, and recent experiments with an injected DFB laser in Refs. [60, 61, 62] showed very good agreement between experiment and theory based on the rate equations (1) over the physically relevant region in the entire (K, ω)-plane. However, even for Fabry-Perrot lasers (simply a lasing material located between two mirrors), which can lase at different modes depending on the operating conditions, the assumption of single mode operation is known to be justified for large regions of the (K, ω)-plane [63]; see also the experiments in Ref. [64].

3. Homoclinic teeth

The phenomena we are interested in appear in what we call 'homoclinic teeth'. What we mean by a homoclinic tooth is sketched in figure 1. It is the region bounded by the curve h^1 of a 1-homoclinic bifurcation and the grey part of the curve S_l of local saddle-node bifurcations. The two curves meet at two points A_1 and A_2 of codimension-two non-central saddle-node homoclinic bifurcations. This codimension-two bifurcation was identified in Ref. [59] as an organizing center for multipulse excitability (single pulse excitability in the case of a curve of 1-homoclinic bifurcations); see Ref. [65, 66, 67] for more details on its unfolding. Figure 1 shows sketches of phase portraits for different locations of parameter space near the homoclinic tooth. Notice, in particular, that the saddle-node bifurcation takes place on a periodic orbit along the parts marked S_g (where g stands for global), but this is not the case along S_l (where l stands for local) .

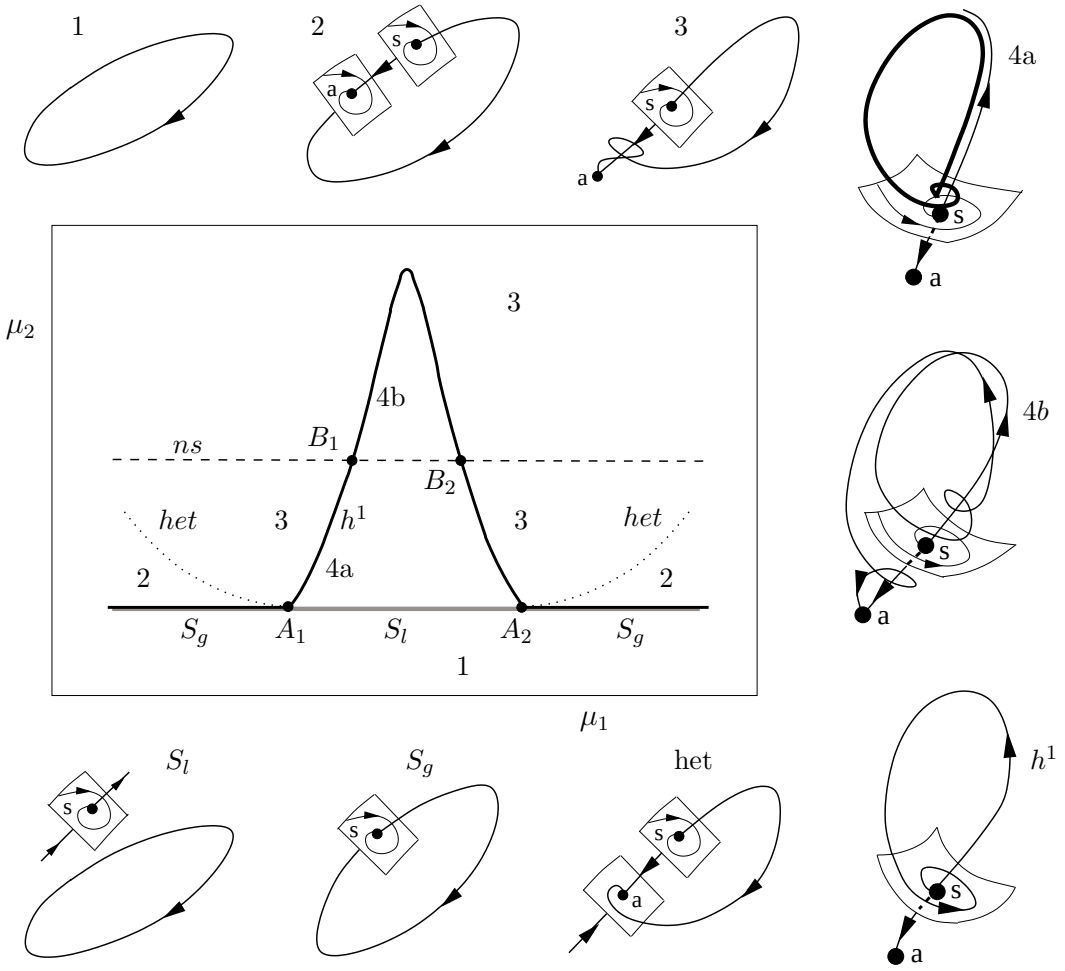

Figure 1. Sketches of phase portraits near the boundary of a homoclinic tooth in two unfolding parameters μ_1 and μ_2.

In the part of region 3 that is close to the curves h^1 and S_g the laser is 1-excitable: a small perturbation to above the stable manifold of the saddle s will lead to a large excursion, essentially following the 1-homoclinic orbit, before the laser relaxes back to the attractor a. By comparison, in region 2 there is a smooth invariant circle, but the laser is still excitable close to the curve S_g: a perturbation beyond the stable manifold of s will lead to a large excursion around the invariant circle and back to a. In fact, phase portraits 2 and 3 are topologically equivalent. However, away from the codimension-two points A, they may relate to different physical phenomena. On the one hand, phase portrait 2 represents phase locking because the smooth invariant circle is centered at the origin of the complex E-plane. Hence, an excitable response associated with phase portrait 2 is mainly of the form of a 2π phase slip with only slight variations in the electric field amplitude. On the other hand, the upper branch of the unstable manifold in phase portrait 3 evolves away from the origin of the complex E-plane so that an excitable response leads to a short (30 ps in our case) and distinct intensity pulse. Near

A, the difference in the excitable response for the phase portraits 2 and 3 disappears. The curve *het* is not a bifurcation curve, but when crossing it there is a change of the direction from which the relevant branch of the unstable manifold of the saddle approaches the attractor. Consequently, the closure of the unstable manifold of the saddle is a smooth curve in region 2, while this is not the case in region 3; see Ref. [59] for more details.

The homoclinic tooth is shown to intersect with the dashed curve ns where the saddle is neutral, that is, the absolute values of the real parts of the real eigenvalue and of the pair of complex conjugate eigenvalues are equal. What the dynamics looks like inside the tooth crucially depends on whether one is above or below ns. Along the parts of h^1 below ns, often called a simple Shil'nikov case, the = homoclinic orbit bifurcates into an attracting periodic orbit [figure 1 = (4a)]. On the other hand, along the parts of h^1 above ns, often called a chaotic Shil'nikov case, the bifurcating periodic orbit is no longer stable [figure 1 (4b)]. Breaking this type of homoclinic orbit leads to the creation of n-homoclinic orbits for any n. While the curve ns is not a bifurcation curve, each of its intersection points B_1 and B_2 with h^1 is a codimension-two homoclinic bifurcation, known as a Belyakov point [69, 70]. Belyakov points mark the transition between the two cases of homoclinic orbits and, hence, give rise to an intricate structure of n-homoclinic orbits; see already figure 4 below.

How homoclinic teeth arise in Eq. (1) is shown in figure 2 with panels of the (K, ω)-plane near the locking region for increasing values of α as indicated. It shows the curves S of saddle-node bifurcations and the curves H of Hopf bifurcations (both shown in gray), the supercritical parts of which bound the locking region of the injected laser; see Ref. [28]. Also shown is the neutral saddle curve ns. All these curves are given by local conditions at equilibria of Eq. (1) and can be found analytically. The curve h^1 of 1-homoclinic bifurcations, on the other hand, cannot be found analytically. It was computed with the HomCont part of the continuation package AUTO [24]. The computations do not distinguish between a generic (codimension-zero) homoclinic connection along the parts S_g in figure 1 and the codimension-one homoclinic bifurcation along h^1. In other words, when the black curve in figure 2 coincides with S then the saddle-node bifurcation takes place on a periodic orbit. If it leaves S we find a homoclinic tooth.

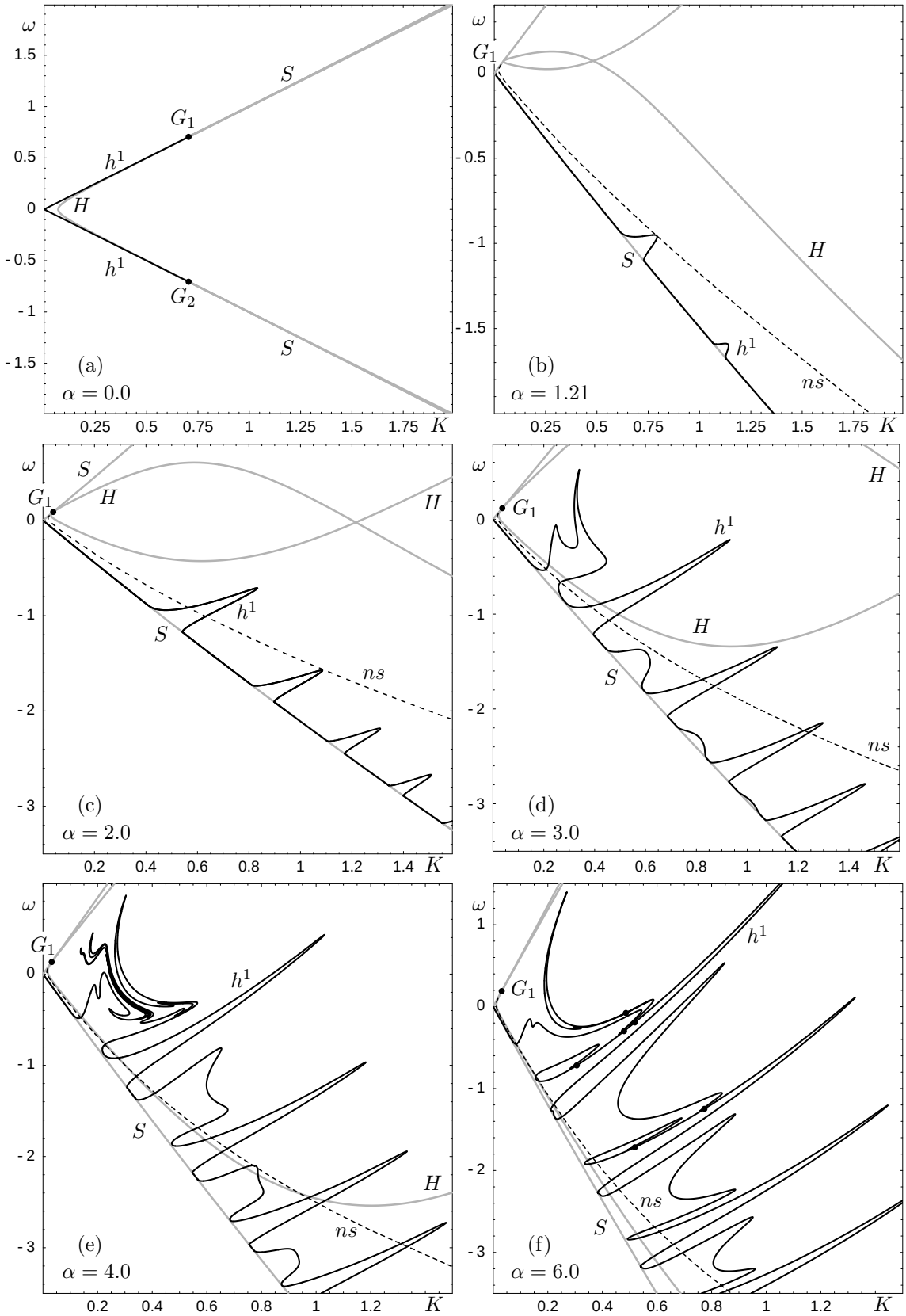

Figure 2. Homoclinic teeth in the locking region as a function of α.

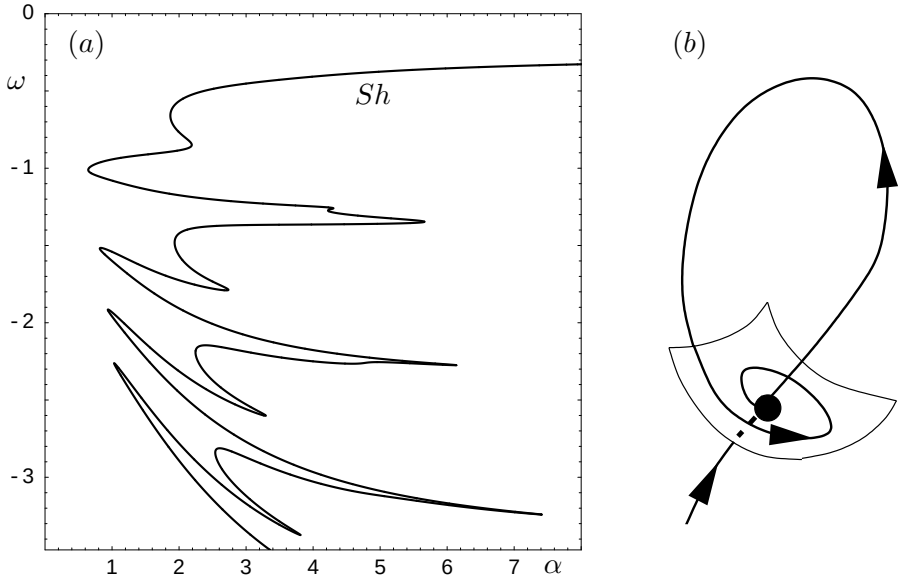

Figure 3. Curve of codimension-two saddle-node homoclinic bifurcations, projected onto the (α, ω)-plane (a), and a sketch of a codimension-two saddle-node homoclinic orbit (b).

For $\alpha = 0$ (the case of a solid-state or CO_2 laser) the (K, ω)-plane is symmetric and there are no homoclinic teeth. As α is increased, homoclinic teeth start to grow along the saddle-node bifurcation curve S that forms the lower boundary of the locking range. (The other boundary is the Hopf bifurcation curve H.) Initially the teeth are quite small [panel (b)] but then they grow in size and the bifurcation diagram changes qualitatively, showing the existence of codimension-three phenomena. At $\alpha = 1.21$ [panel (b)] the first tooth starts to intersect the neutral saddle curve ns. What is more, new teeth start to appear between already present teeth [panel (d)]. All teeth keep growing, and the tooth closest to the saddle-node Hopf point G_1 develops a rather bizarre shape [panels (e) and (f)]. On top of this, when α increases neighboring teeth may merge, meaning that the curve h^1 detaches from the curve S. This occurs at codimension-three points when two neighboring non-central saddle-node homoclinic bifurcation points come together and vanish. Furthermore, one notices the appearance of codimension-two homoclinic bifurcation points (dots along the curve h^1 in panel (f)). They are created when the section given by fixed α crosses a minimum in the respective codimension-two bifurcation curve, which is discussed in detail in section 5.

To study how new teeth are born and neighboring teeth merge we continued with HomCont the curve of codimension-two non-central saddle-node homoclinic bifurcations in (K, ω, α)-space [67, 68]. The projection of this curve onto the (α, ω)-plane is shown in figure 3(a), while figure 3(b) shows a sketch of a non-central saddle-node homoclinic orbit. The left-hand fold points of the curve in figure 3(a) are points where teeth are born, while right-hand fold points are points where two neighboring teeth merge. This

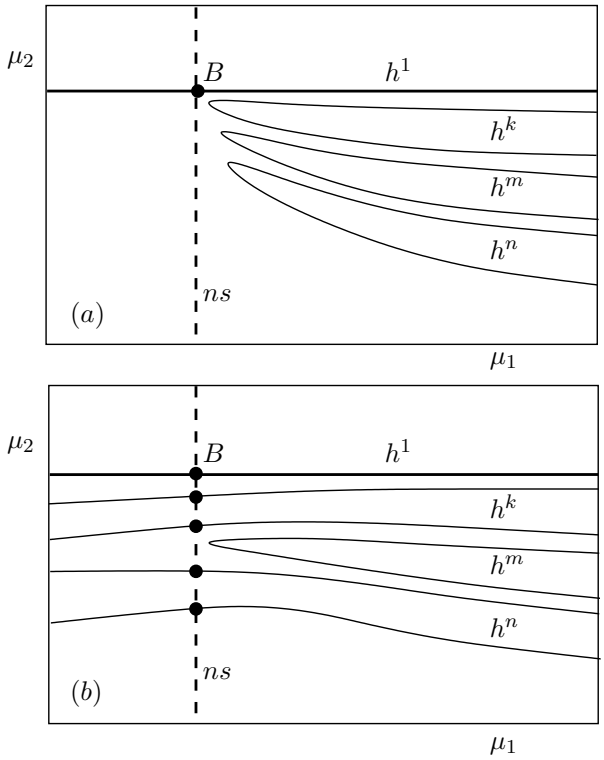

Figure 4. Sketches of the two types of Belyakov points, as described in Ref. [69].

figure clearly shows that there are no teeth for $\alpha < 0.5$. New teeth are then born one-by-one as α is increased. Secondary teeth appear from about $\alpha = 2$ on. Merging teeth can be observed from about $\alpha = 2.2$ onward when the first two teeth (nearest G_1) merge. Successively teeth for larger negative detuning ω also merge. In fact for $\alpha > 7.5$ there appears to be one giant tooth, if one still wants to call it that. It is already clear that the situation becomes increasingly complicated with α.

4. Complex structure of n-homoclinic bifurcations

Complex structures of global homoclinic and heteroclinic bifurcations arise inside the homoclinic teeth as a result of interactions of the curves of 1-homoclinic orbits. The fact that the curve ns intersects the first homoclinic tooth, for example, for $\alpha = 2.0$ in figure 2 (c), giving rise to two Belyakov points, already allows us to conclude from general theory [69, 70] that there must be further curves of n-homoclinic orbits. In figure 4 we plot two possible (partial) bifurcation diagrams near a Belyakov point B as described in Ref [69]. In panel (a) the point B is accumulated on one side by curves of n-homoclinic orbits, while in panel (b) certain curves of n-homoclinic orbits pass close to the point B. In either case, the Belyakov point B gives rise to n-homoclinic orbit for any n. We remark that the exact combinatorics of these n-homoclinic orbits is still not fully understood [70].

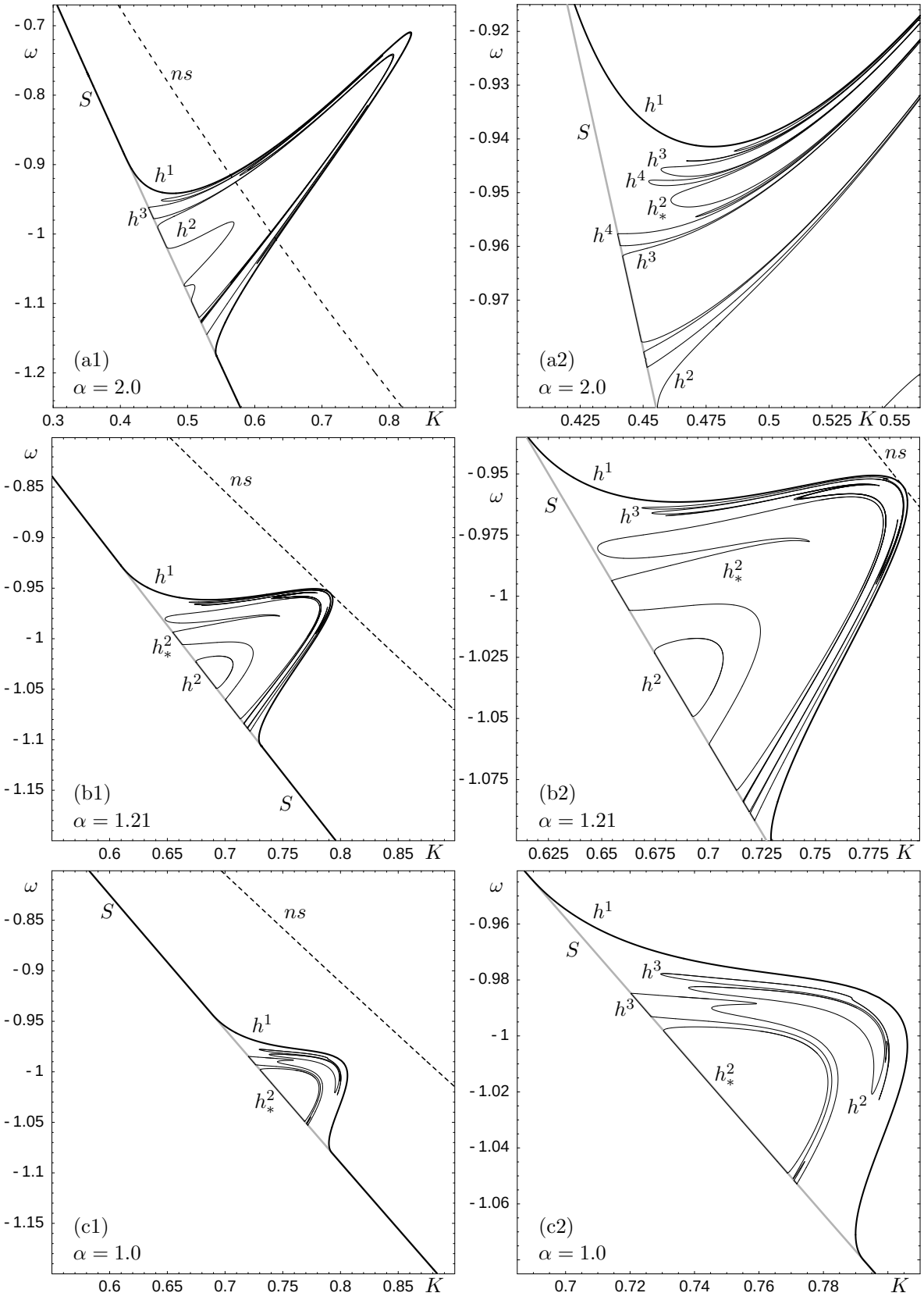

Figure 5. Bifurcation curves of n-homoclinic orbits inside a homoclinic tooth for three different values of α as indicated in the panels.

The question is how these n-homoclinic orbits are organized inside the homoclinic teeth. At the same time, this gives an impression of a Belyakov bifurcation in a concrete system. Furthermore, one may ask where the associated n-homoclinic bifurcation curves go and to which other codimension-two points they connect. In short: what is the bifurcation diagram, as far as one can assemble it? These questions cannot be addressed by analytical studies in a neighborhood = near codimension-two points but they require using continuation techniques. From a bifurcation theory point of view, this is the next step towards the understanding of the organizing properties of global bifurcations. Physically, we reveal structures that stretch over large regions in the parameter plane and become experimentally accessible, that is, potentially relevant for real applications of optically injected lasers.

Figure 5 (a1) shows curves h^n of n-homoclinic orbits for $n \leq 4$ inside the first tooth for $\alpha = 2.0$, while figure 5 (a2) is an enlargement near the saddle-node bifurcation curve S. Many of these curves extend from the region above ns to below ns and in crossing ns have further Belyakov points on them. The picture that emerges is that of a complicated arrangement of nested n-homoclinic bifurcation curves. Most interestingly, several curves extend to very near the curve S, and some even attach to S at points of non-central saddle-node n-homoclinic orbits.

We now focus on what happens to the infinite number of h^n-tongues when the Belyakov points are gone, that is, the homoclinic tooth is entirely below ns. One straightforward scenario would be that all the h^n curves disappear when B_1 and B_2 merge. However, this is not the case here. Figure 5 (b1)–(b2) shows the first tooth for $\alpha = 1.21$, just as it touches the curve ns. This is a codimension-three phenomenon in (K, ω, α)-space where two Belyakov points coincide and then disappear when α is decreased, as is shown in figure 5 (c1)–(c2). (The curve B of Belyakov points in (K, ω, α)-space has a minimum.) Even though the tooth is well below the curve ns for $\alpha = 1.0$, there are still curves of n-homoclinic orbits inside it. In particular, we find that the curves h^2 and h^3 are attached to S.

Our numerical investigation suggests that there are only finitely many curves of n-homoclinic orbits for $\alpha < 1.21$. To illustrate how subsequent curves h^n appear with increasing α we marked one of them with a star. For $\alpha = 1.0$ [figure 5 (c2)] h^2_* is the last homoclinic curve that just emerged from the saddle-node bifurcation curve S. As α is increased above $\alpha = 1.0$, the curve h^2_* develops two = extra noncentral-homoclinic points on S, forms a sort of bridge, and provides space for the next homoclinic curve to emerge [figure 5 (b2)]. This process seems to repeat, such that for $\alpha > 1.21$ there exist infinitely many curves h^n.

The regions bounded by h^2 and h^3 near S appear to be large enough to be experimentally accessible [51]. In such a region the laser exhibits multi-pulse excitability. We remark that our study shows that this phenomenon can be found even for surprisingly low values of α; compare Ref. [9, 59]. An example is shown in figure 6 for $\alpha = 1.0$. The phase portrait in figure 6 (a1) is as that of region 3 in figure 1 — the laser is 1-pulse excitable. A small perturbation above the excitability threshold, given

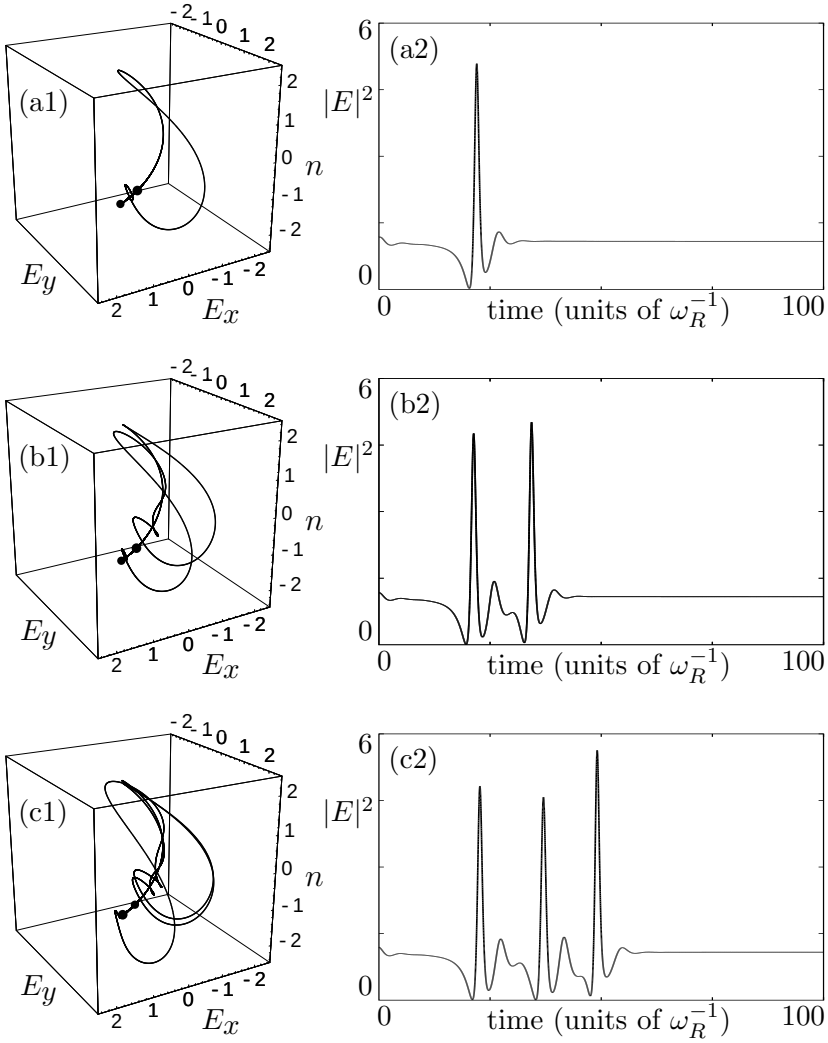

Figure 6. Examples of multi-pulse excitability. The left column shows the phase portrait and the right column the reaction of the laser to a small perturbation above the excitability threshold. Throughout $\alpha = 1.0$ and from (a) to (b) (K,ω) takes the values $(0.71, -0.95)$, $(0.745. - 1)$ and $(0.735, -0.993)$.

by the stable manifold of the saddle point, results in the laser sending out a single pulse; see figure 6 (a2). In the region bounded by h^2, on the other hand, the phase portrait is close to a 2-homoclinic orbit and the laser produces two pulses in reaction to a single perturbation; see figure 6 (b1)–(b2). Finally, three pulses result in the region bounded by the curve h^3, as is illustrated in figure 6 (c1)–(c2). Indeed, it is possible to find n-pulse excitability for any n, but the regions for $n > 4$ become impractically small.

It is important to note a key ingredient for multipulse excitability to occur, namely the fact that the respective curve h^n extends all the way below ns. For the parameters above ns the h^n-tongues are so narrow that they become hard to distinguish, even

numerically. Furthermore, there exist an infinite number of unstable periodic orbits in the phase space for parameters outside the tongues. As a result, the excitable response is often irregular and unpredictable as the trajectory bounces between the unstable orbits before it decides to return to the stable equilibrium. On the other hand, below ns the tongues are easily distinguishable and the phase portraits are simpler as there are no unstable periodic orbits. Consequently, the system can be prepared to be well within h^n (certainly for $n \leq 3$) where the excitable response is predictable and consist of a certain number of pulses.

5. Codimension-two homoclinic bifurcations

We now study in considerable detail the structure and bifurcations of the curve h^1 that forms the boundary of the homoclinic teeth. In particular, we show that codimension-two double-homoclinic and T-point bifurcations play a prominent role in organizing the dynamics.

Figure 7 shows an enlargement near the first homoclinic tooth (or what is left of it) for $\alpha = 4.5$; compare with figure 2. Notice the two points D_1 and D_2 where additional homoclinic bifurcation curves emerge. The phase portraits at D_1 and D_2 show that we are dealing with a codimension-two *double-homoclinic orbit* [18, 21]: both branches of the unstable manifold spiral back to the saddle point. This means that there are simultaneously two individual homoclinic orbits associated with the same saddle point.

The two phase portraits at D_1 and D_2 are topologically equivalent and both lie on the primary branch of the curve h^1. This can be seen in the further enlargement of the (K, ω)-plane in figure 8, where panels (a)-(e) show the 1-homoclinic orbit in phase space at the indicated parameter points along h^1. As D_2 is approached the unstable manifold forming a homoclinic orbit comes closer and closer (from below) to the saddle and then leaves a neighborhood of the saddle roughly along the other branch of the unstable manifold. Finally, at D_2 there are two simultaneous homoclinic orbits, one for each branch of the unstable manifold. Effectively, the original 1-homoclinic orbit along the curves h^1 has split into two homoclinic orbits. Notice that the curve h^1 accumulates back on itself at D_2, as is also sketched in the inset of figure 8.

This scenario agrees with what is known in the literature about the double-homoclinic bifurcation [18, 21]. Again, not all details of this codimension-two global bifurcation are known, but key features are as sketched in figure 9 (for the case of a saddle focus as we encounter it here). The double-homoclinic orbits D exists at the intersection point of two curves h^1_a and $\tilde{h}^1$ of two different homoclinic orbits to the same saddle that contain each a different branch of the unstable manifold of the saddle. As sketched, there is a third curve h^1_b of homoclinic orbits that accumulates on the curve h^1_a. The accumulation is as shown when the saddle quantity is larger than one [18, 21], which is the case we encounter, because all double-homoclinic orbits occur above the curve ns.

Note that the analysis in the literature is in terms of a small tubular neighborhood

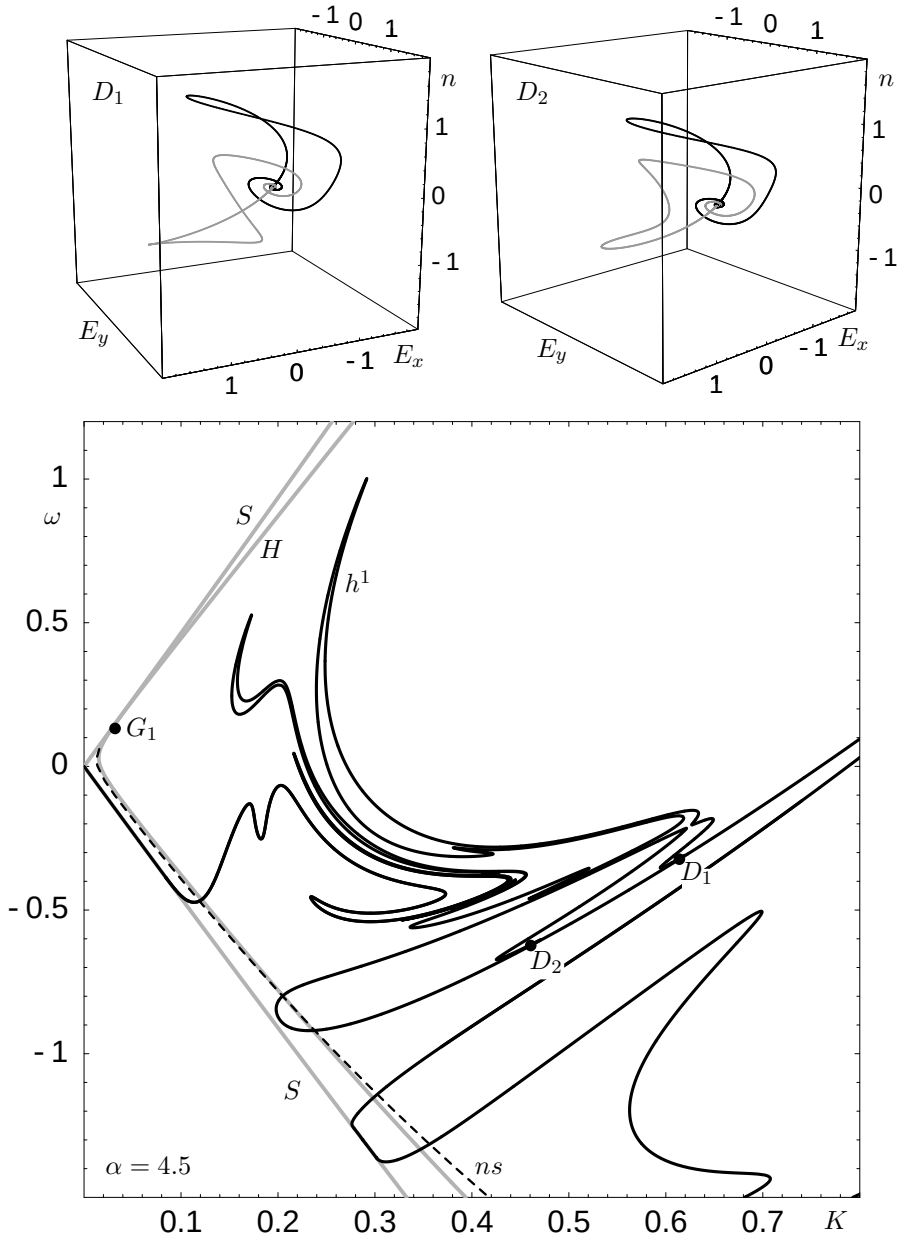

Figure 7. The (K, ω)-plane for $\alpha = 4.5$ near the point G_1 (compare with figure 2) and the phase portraits at the codimension-two double-homoclinic bifurcation points D_1 and D_2.

around the double-homoclinic orbits as sketched in panel D. In this neighborhood the curves h_a^1 and h_b^1 are unrelated. However, as can be seen in figure 8, they may be one and the same curve accumulating back on itself. In fact, we find this to be the typical situation in system (1). We finally stress that the points D_i that we encounter in this work are of codimension-two because the two simultaneous homoclinic orbits are not related by symmetry. Unlike in the case of codimension-one symmetric double-

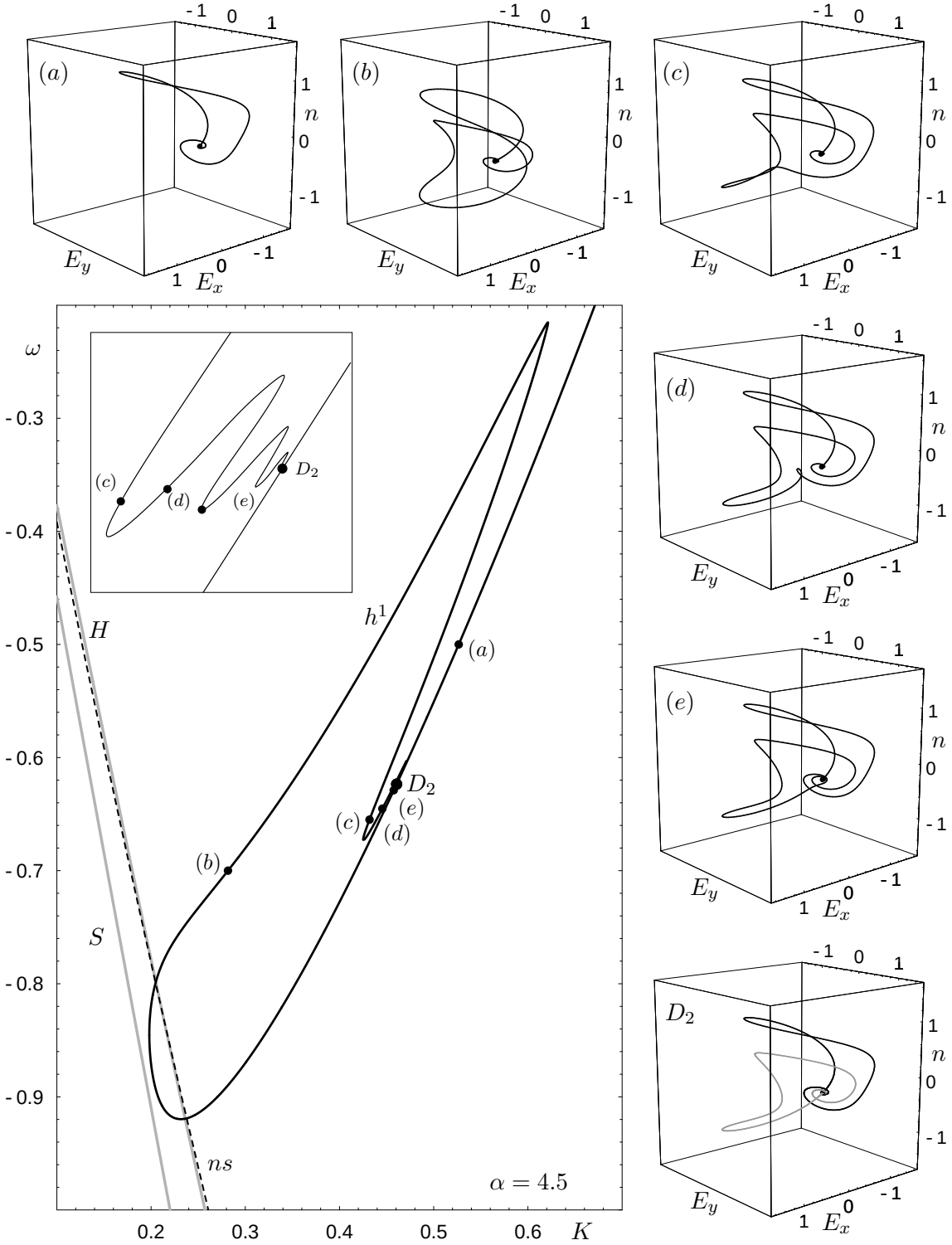

Figure 8. The (K, ω)-plane for $\alpha = 4.5$ near the point D_2 (compare with figure 7) and the phase portraits along the homoclinic curve h^1 as D_2 is approached.

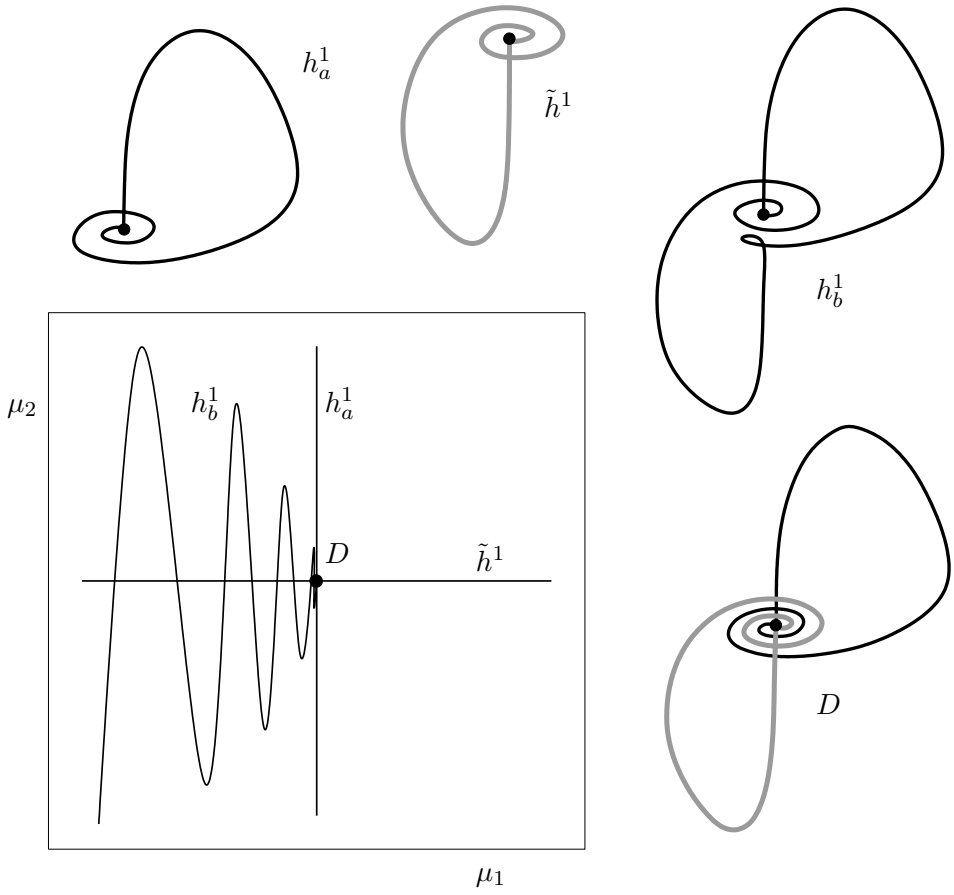

Figure 9. Sketch of phase portraits and the bifurcation diagram (in two unfolding parameters μ_1 and μ_2) of a double-homoclinic point D, as described in Refs. [18, 21].

homoclinic orbit, it is possible to perturb parameters such that one of the homoclinic connections is broken but the other is not.

In figure 7 and figure 8 we found the double-homoclinic points D_1 and D_2 as the end points of the curve h^1 as it accumulates on itself. However, we know from figure 9 that there must be a curve $\tilde{h}^1$ of a second homoclinic orbit crossing at D_i. In order to find this new homoclinic orbit we split off the new homoclinic orbit from the data of the approximate double-homoclinic orbit at D_i (given as the end point of the curve h^1). We then follow this second codimension-one homoclinic orbit in the (K, ω)-plane.

The result is shown in figure 10. The point D_2 is indeed the intersection point of two curves of codimension-one homoclinic orbits. The new curve $\tilde{h}^1$ also contains D_1 and has two end points. One end point is the point D_3 of a double-homoclinic orbit, which lies on the curve $\tilde{h}^1$ itself. The other end point is a point denoted by T_1 that is reached in a spiraling fashion, as is also sketched in the inset.

At the point T_1 we encounter a bifurcation that is generally referred to as a *T-point bifurcation*. This type of codimension-two heteroclinic cycle was studied in a general

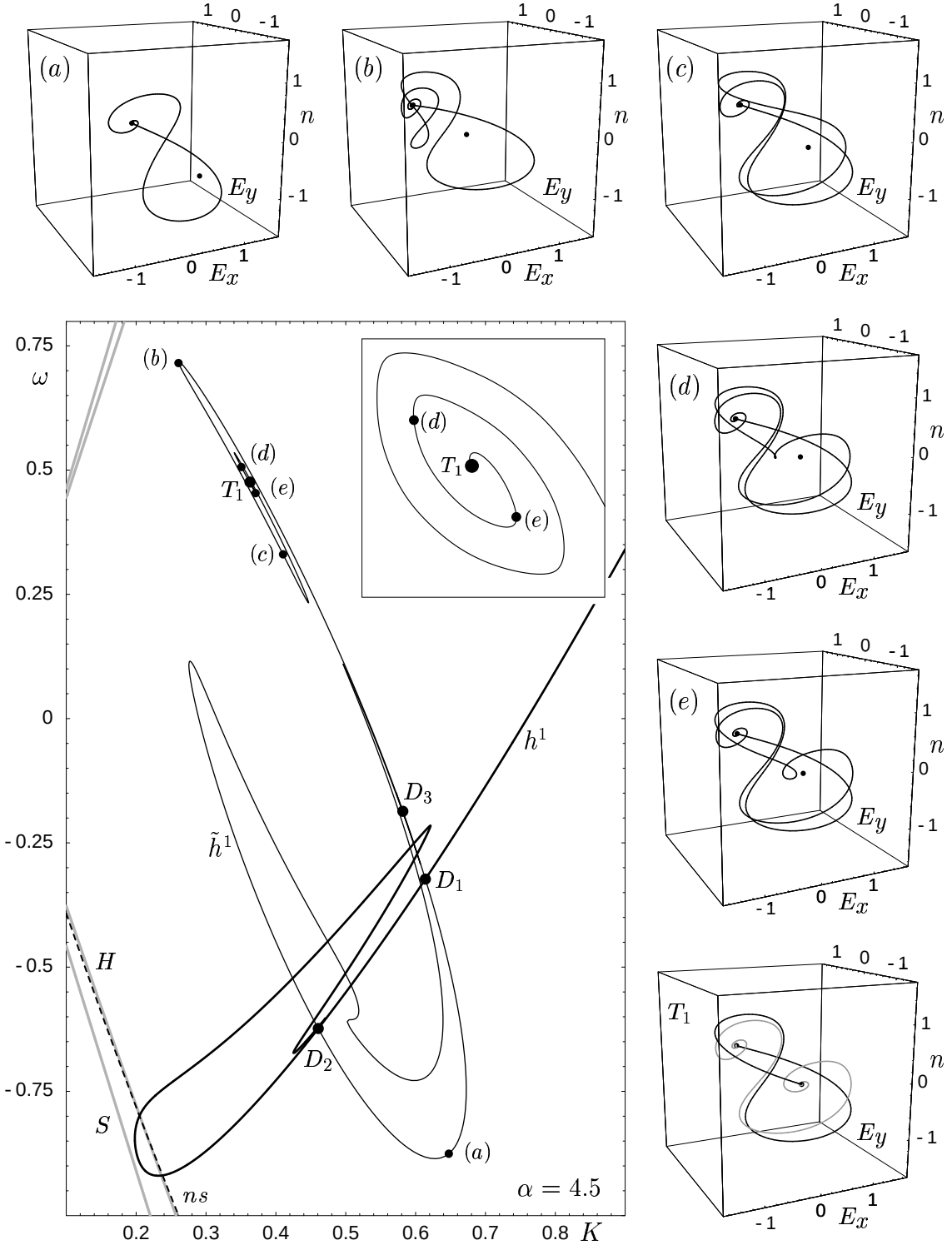

Figure 10. The (K, ω)-plane for $\alpha = 4.5$ near the points D_1, D_2, D_3, and T_1 with phase portraits as T_1 is approached.

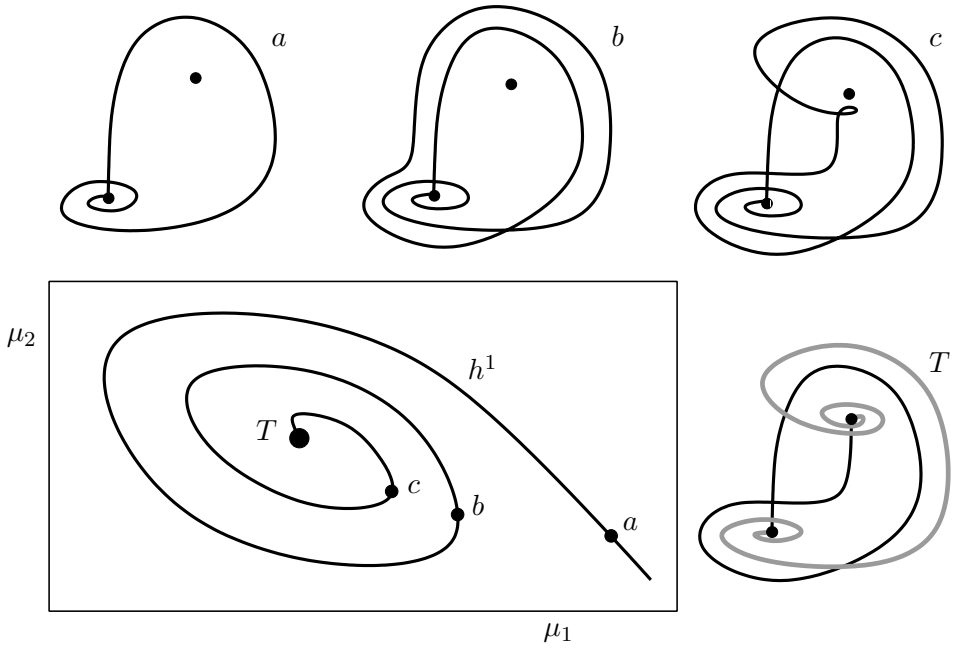

Figure 11. Sketches of the phase portraits along the homoclinc bifurcation curve approaching a T-point in the plane of two unfolding parameters μ_1 and μ_2.

system, that is, one without any symmetry, in Ref. [17, 18] in a tubular neighborhood around the heteroclinic orbits at the T-point. Note that the T-point bifurcation is often associated with vector fields that have the $\mathbb{Z}_2$-symmetry of a rotation by π around an invariant axis. In this case, the heteroclinic cycle involves two saddle-foci, which are each others images under the symmetry, and the origin (more generally, a point in the invariant subspace of the symmetry), which is also a saddle-focus. This $\mathbb{Z}_2$-symmetric T-point bifurcation was initially found and studied in the Lorenz system [11], but also occurs in other systems with rotational symmetry, such as an optically pumped three-level laser [12], an electronic oscillator [13], and a semiconductor laser with phase-conjugate feedback [14]. It was recently also discovered in systems with the $\mathbb{Z}_2$-symmetry of point-reflection [15, 16].

What we find is a general T-point bifurcation (that is, in a system without symmetry) for the case that both saddles involved are saddle foci. The approach to the point T is illustrated in figure 10 (a)-(e) with images of the 1-homoclinic orbit in phase space at the indicated parameter points along the curve $\tilde{h}^1$.

The situation (a part of the bifurcation diagram near a T-point) is sketched in figure 11. As the point T is approached along h^1, the homoclinic orbit approaches a second saddle focus, passing closer and closer by the saddle. At the point T_1 there are two heteroclinic connections: a codimension-two heteroclinic connection (black) where the one-dimensional unstable manifold of the first saddle coincides with the one-

dimensional stable manifold of the second saddle, and a generic (codimension-zero) heteroclinic connection (gray), given as the intersection curve of the two-dimensional stable manifold of the first saddle and the two-dimensional stable manifold of the second saddle.

According to general theory [17, 18] there must exist a second spiraling curve of homoclinic connection to the other (lower) saddle, leading to another curve in parameter space that spirals into T_1. Furthermore, it is known that there are many more curves of n-homoclinic bifurcations, which pass close to the saddles an arbitrary number of times. We did not attempt to find all these bifurcation curves, but instead concentrated on the structure of 1-homoclinic bifurcation curves. Nevertheless, the injection laser appears to be a good model in which to study global bifurcations near T-point bifurcations in more detail.

The bifurcation diagram in figure 10 is still quite incomplete. The curve $\tilde{h}^1$ of homoclinic orbits also accumulates on itself at D_3. So, as we did near the double-homoclinic point D_1, we find and follow the second codimension-one homoclinic that must exist near D_3. This gives the continuation of the curve h^1 shown in figure 12, which ends at the point D_1. Furthermore, we followed from near T_1 the codimension-one homoclinic orbit of the (upper) saddle point to lower values of α (see already figure 13), where we discovered a second T-point bifurcation T_2. We then followed this T-point back to $\alpha = 4.5$. As can be seen in figure 12, the point T_2 is the end point of two spirals. In fact both spirals turn out to belong to one and the same closed curve $\tilde{h}^2$ of codimension-one two-homoclinic orbits as is illustrated by the sketch in the inset.

The bifurcation diagram in figure 12 is quite intricate: it involves several double-homoclinic and T-point bifurcations. Unraveling it required detailed numerical continuation with HomCont, guided by theoretical knowledge of which homoclinic orbits are possible near the different codimension-two points. We finally remark, that figure 12 shows a 'skeleton' consisting of curves of 1-homoclinic bifurcations. Indeed the existence of the T-points suggests that there are n-homoclinic orbits for arbitrary n.

6. Folds of codimension-two homoclinic bifurcation curves

We know from figure 2 that the complicated structure of codimension-two bifurcations in figure 12 is not present for smaller values of α. The question arises of how it disappears.

It turns out that an important ingredient in this change of the bifurcation diagram are minima (more generally, folds) with respect to α of certain curves of codimension-two homoclinic bifurcations in the three-dimensional (K, ω, α)-space. This phenomenon is of codimension three, where one codimension is due to the fold, which is the basic singularity of a curve in the three-dimensional parameter space. The other two codimensions are due to the special object in phase space, in this case a codimension-two homoclinic bifurcation. One might speak of a codimension-two-plus-one event to distinguish it from codimension-three bifurcations, where all codimensions are due to a codimension-three object in phase space.

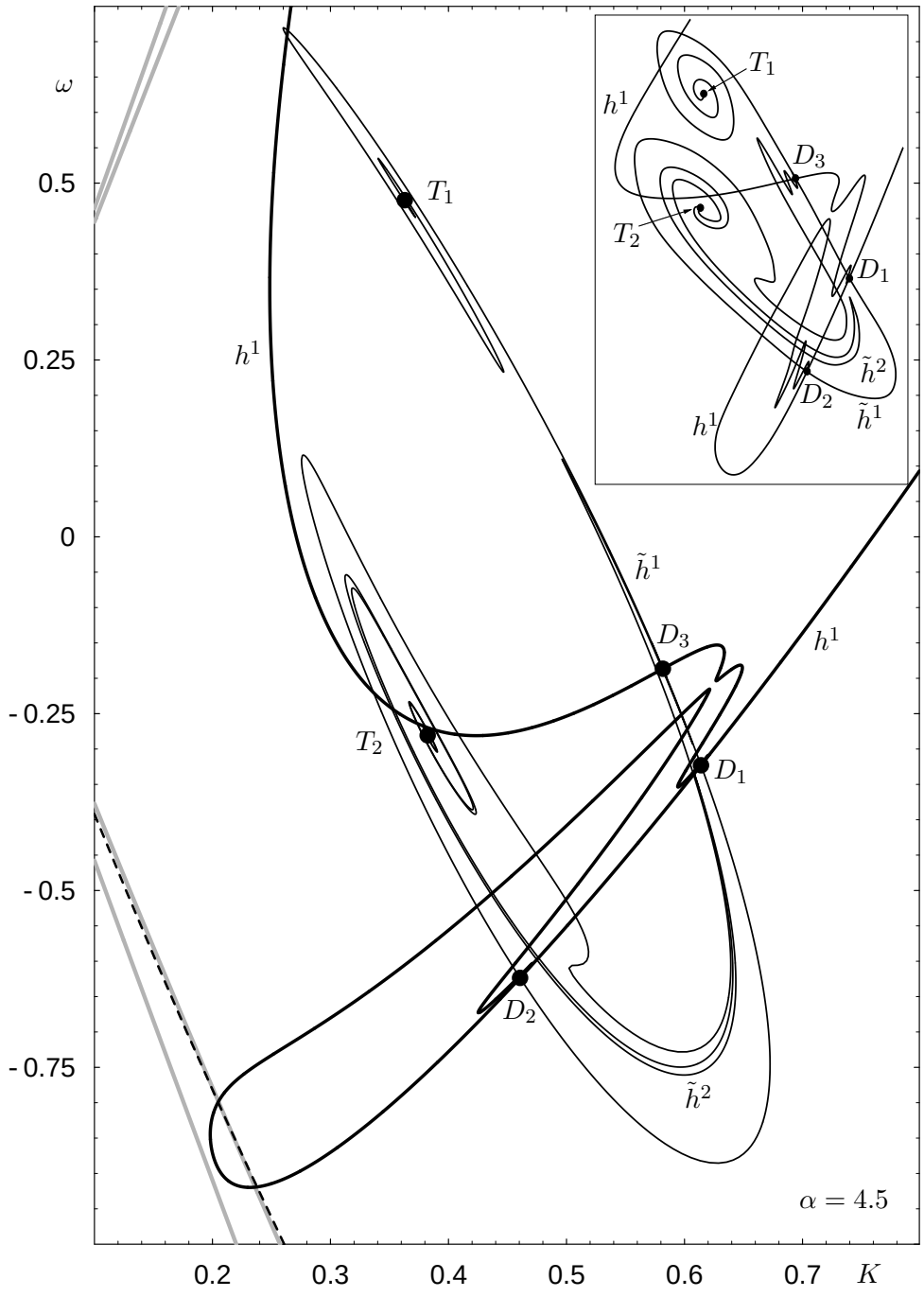

Figure 12. The (K, ω)-plane for $\alpha = 4.5$ near the points T_1 and T_2.

We already encountered this phenomenon in the creation and disappearance of points of codimension-two saddle-node homoclinic bifurcation (see the folds with respect to α in figure 3) and in the creation, with increasing α, of Belyakov points in the tangency between the curves ns and h^1 (see figure 5). In this section we consider two

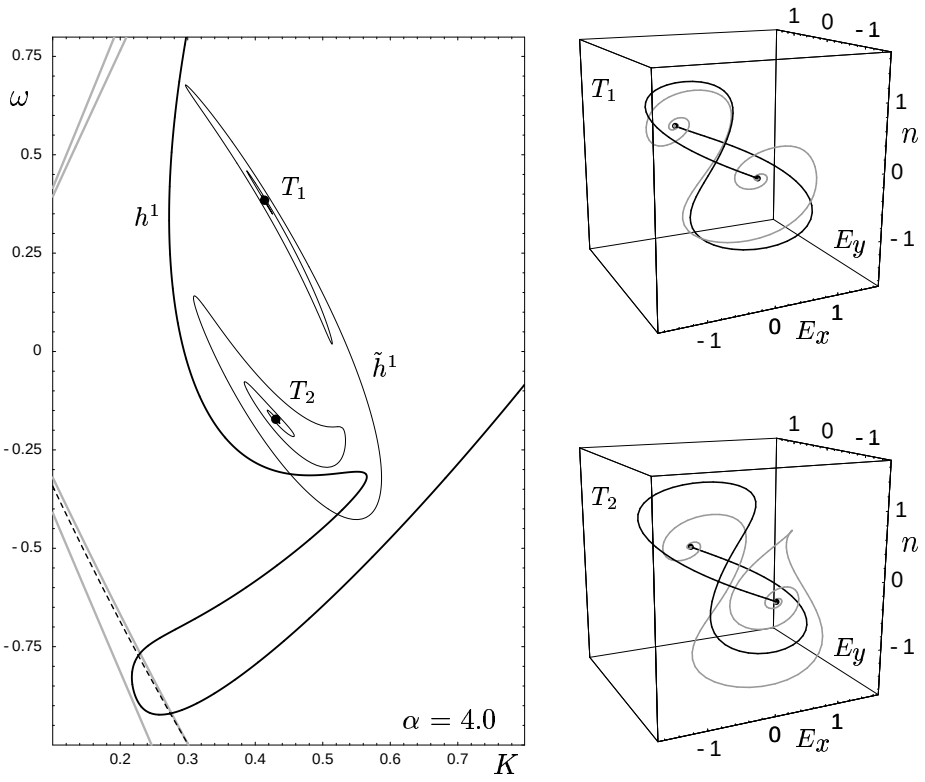

Figure 13. The (K, ω)-plane for $\alpha = 4.0$ near the points T_1 and T_2 and the respective phase portraits at T_1 and T_2.

other examples, namely a fold of a curve of T-point bifurcations and a fold of a curve of double-homoclinic bifurcations. As we will see now, in both these examples the fold of the codimension-two curve is accumulated by singularities of associated surfaces of codimension-one global bifurcations.

We first consider the case of T-point bifurcations. Figure 14 shows what happens to the points T_1 and T_2 as α is decreased. After the disappearance of the point D_3, the points T_1 and T_2 move closer and closer to each other. There are a number of codimension-three events where the spiral around T_1 touches that around T_2. Each such event leads to a new closed curve surrounding both T_1 and T_2 and the curve of homoclinic orbits connecting T_1 and T_2, as in figure 14 (c). This process continues until the points T_1 and T_2 finally coincide, leaving behind a number of closed concentric curves of homoclinic orbits, as in figure 14 (d). These closed curves then disappear one by one as α is decreased further. (We remark that this phenomenon has been found independently in Ref. [15] in the $\mathbb{Z}_2$-symmetric Chua's circuit with a cubic nonlinearity.) Finding this transition numerically was quite a challenge because the curves involved are no longer connected. We succeeded by starting from suitable points and continuing the respective homoclinic orbit in α.

The individual changes in the structure of the curve $\tilde{h}^1$ are due to a classical

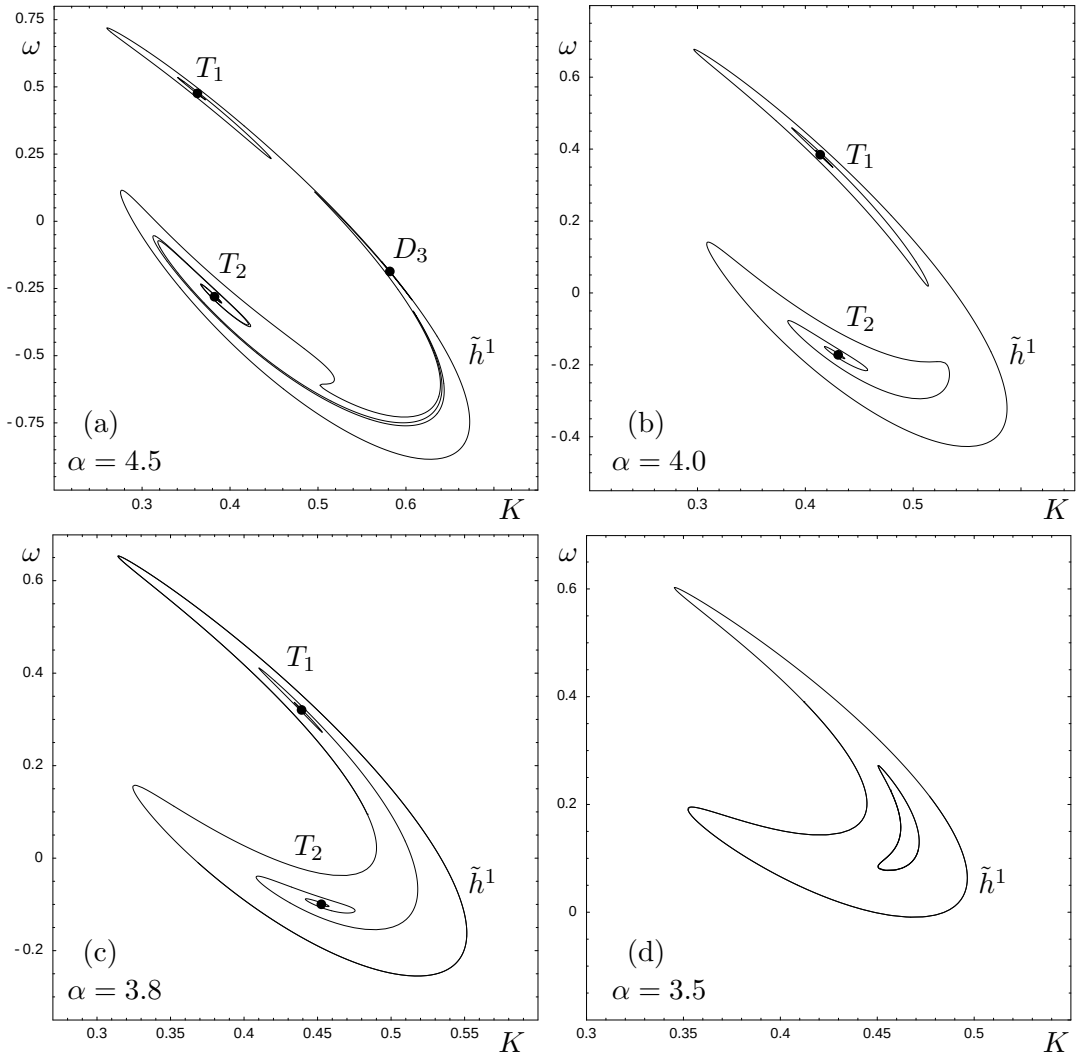

Figure 14. Dependence on α of the (K, ω)-plane near the points T_1 and T_1.

singularity, namely the passage trough an α-degenerate point. At such a point, the tangent space to the $\tilde{h}^1$ surface in (K, ω, α)-space does not have an α-component (the derivative with respect to α is zero). There are two cases depending on the index of the α-degenerate point, namely the transition trough a saddle and the transition through an extremum. Both are sketched in figure 15. Note that these singularities are also called the simple bifurcation and the isola bifurcation; see, for example, [72] for details.

This explanation in terms of singularity theory is a consequence of the geometry of bifurcation surfaces and curves in (K, ω, α)-space. In fact, the whole sequence of events of T_1 and T_2 coming together and disappearing can be nicely explained with the sketch in figure 16 of how the surface $\tilde{h}^1$ of homoclinic bifurcations spirals around the curve T of T-point bifurcations. The curve of T-point bifurcations is a smooth curve with a minimum with respect to α, and it is surrounded by a surface of codimension-one homoclinic bifurcations that spirals towards this curve. The panels in figure 14 are

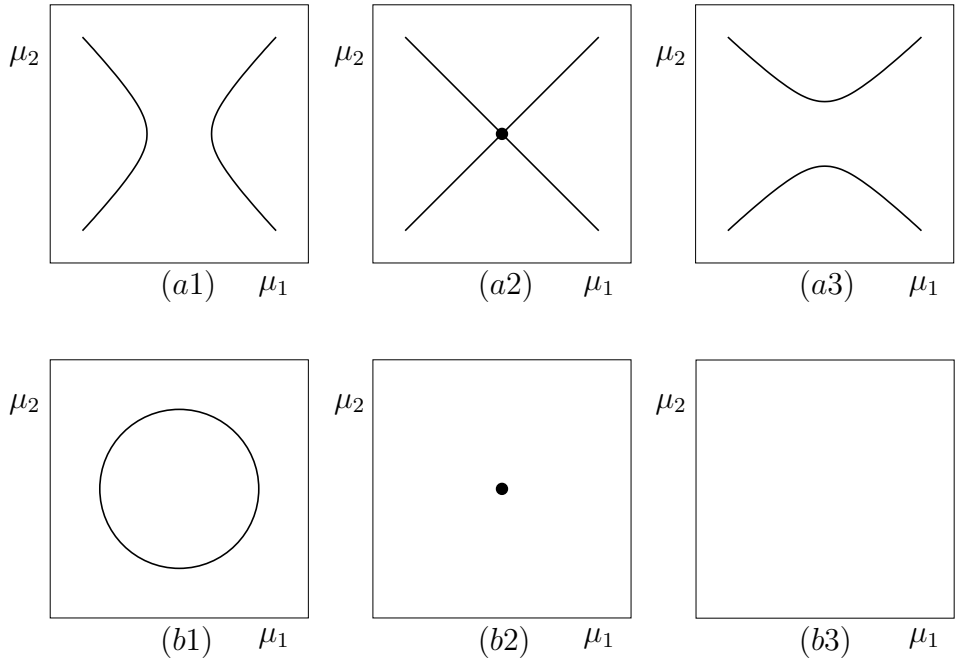

Figure 15. The two codimension-one singularities as a two-dimensional cross section (here parametrized by μ_1 and μ_2) moves through a two-dimensional surface in $\mathbb{R}^3$ are the transition through a saddle point (a) and through an extremum (b).

two-dimensional cross sections for fixed α through this surface. If α is large enough, the curve T is intersected in two points T_1 and T_2 and the spiraling near these two points must be clockwise and counter-clockwise, respectively. The intersection of the surface with the section is a single curve for sufficiently large α. However, nearer the minimum of the curve T the surface has α-degenerate points where its tangent space does not have an α-component. Passing through each such point constitutes a basic codimension-one singularity of the surface of homoclinic bifurcations as sketched in figure 15. More precisely, above the minimum of the curve T there are infinitely many passages through saddles, which accumulate on the minumum of the curve T. Globally, this creates the closed concentric curves by connecting the respective homoclinic curves in a different way. Below the minimum of T, on the other hand, each concentric circle disappears by contracting to a single point, which is the passage through an extremum (with respect to a parameter, in this case α) in a two-dimensional surface $\tilde{h}^1$. We finally remark that it would be quite a challenge to produce a numerical picture of the surface sketched in figure 16.

Our second example is the merging and disappearance of the points D_1 and D_2 as α is decreased from $\alpha = 4.5$ to $\alpha = 4.0$. Figure 17 shows four numerical bifurcation diagrams in this transition. As the points D_1 and D_2 are moving closer together we again encounter a passages through saddle points [see figure 15(a)]. This happens between panels (a) and (b) of figure 17 and it leads to a change in how the curves h^1 in the cross

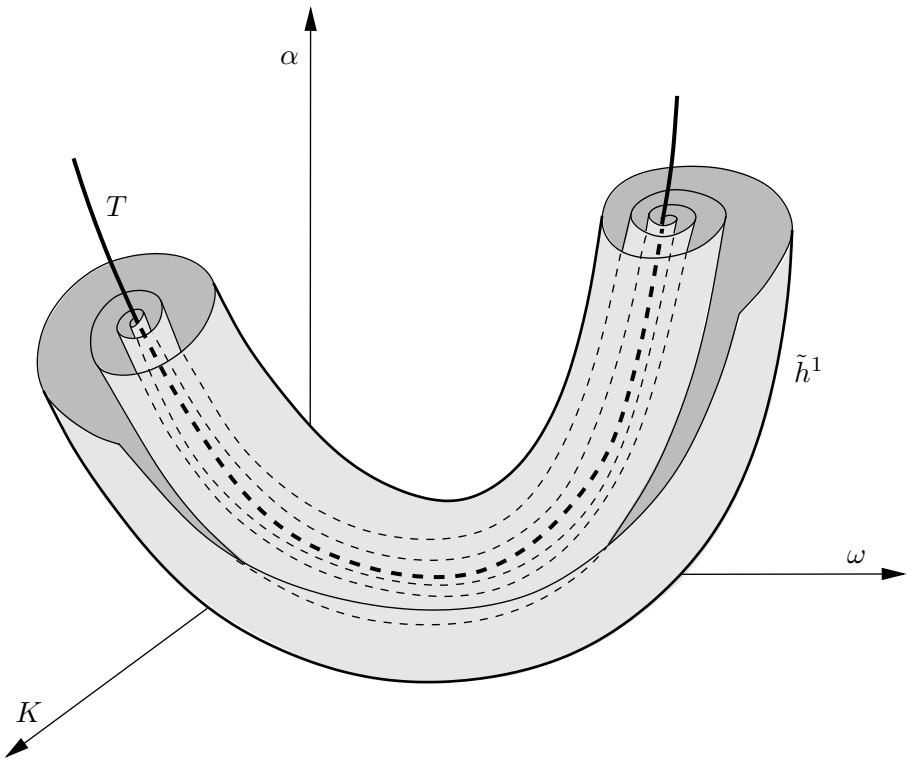

Figure 16. In the (K, ω, α)-space the curve of T-point bifurcation is surrounded by a surface of homoclinic bifurcation $\tilde{h}^1$ that spirals onto the T-curve; compare with figure 14.

section in the (K, ω)-plane connect. After this event, a single curve h^1 connects the two pionts D_1 and D_2 (figure 17(b)). In a further passage through a saddle point the curve h^1 pinches off to create an isola, which is the situation shown in figure 17(c). In fact, the isola is very close to the new connection between D_1 and D_2. Numerical continuation suggests that more and more isolas are formed as D_1 and D_2 come closer together. These isolas then disappear in passages through minima as sketched in figure 15(b). Furthermore, α passes through the minimum of the D curve in the (K, ω, α)-space. As a result, the curves $\tilde{h}^1$ and h^1 in figure 17(d) no longer intersect and the points D_1 and D_2 have disappeared.

To clarify the situation, we sketch the transition leading to the disappearance of D_1 and D_2 in figure 18. It can again be understood by the geometry of bifurcation surfaces in (K, ω, α)-space, which in this case are organized around a minimum (with respect to α) of the curve D of double-homoclinic bifurcations. Figure 18(a)–(c) and (f) are topologically as the numerical bifurcation diagrams in figure 17(a)-(d), respectively. We remark that it becomes more and more difficult to resolve numerically the different, small and disjoint intersection curves of the surface h^1 in (K, ω, α)-space. The sketches in figure 18(d) and (e) are based on our numerical investigations, and indicate how the transition appears to take place. However, the exact details, in particular, the order

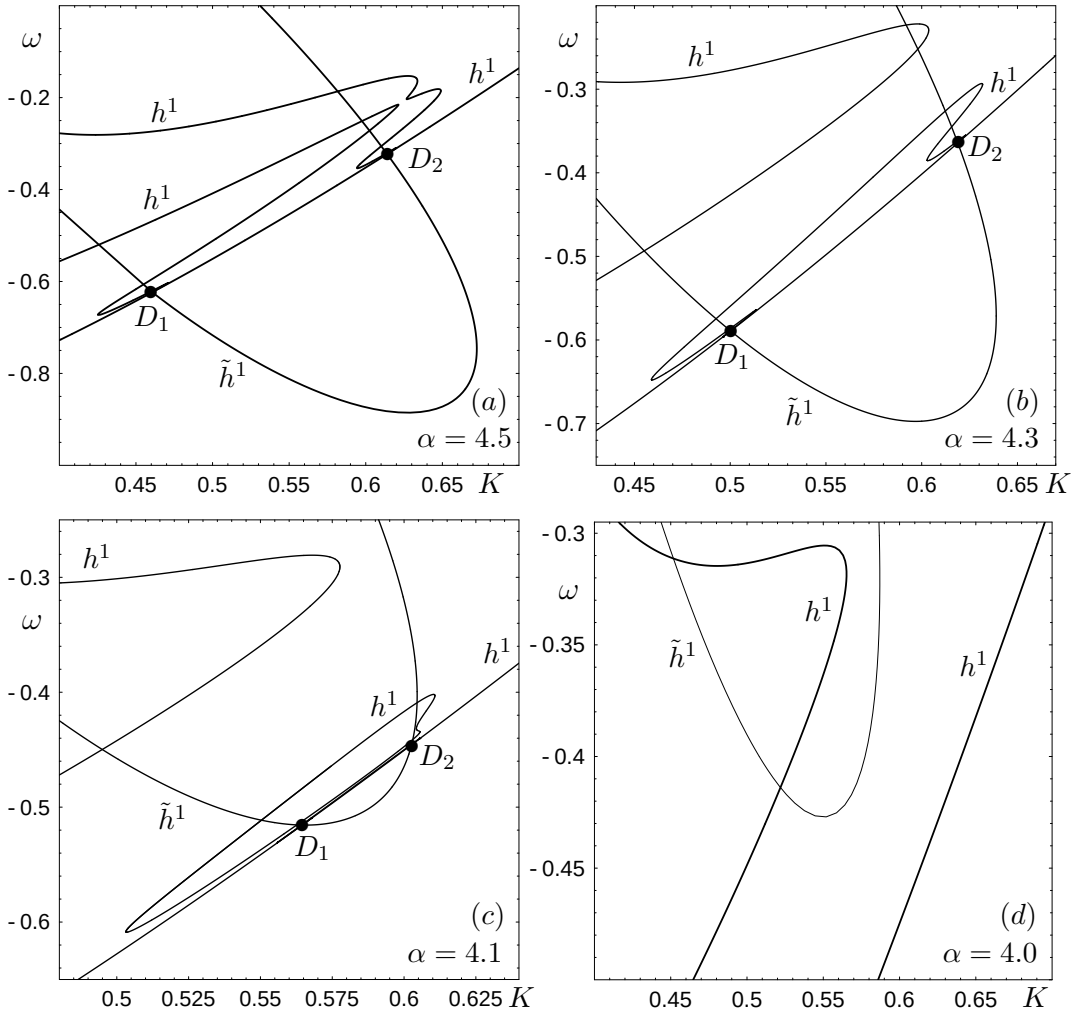

Figure 17. The (K, ω)-plane near D_1 and D_2 for varying α.

in which isolas are created and shrink to points and disappear is yet unknown. Our continuation study suggests the basic ingredients of this transition and can reveal some of the first steps in the specific transition at hand. This scenario agrees with what is known about the (local) codimension-two bifurcation diagrams near a double-homoclinic bifurcation as sketched in figure 9, but a complete study of this codimension-two-plus-one phenomenon remains a challenge beyond the scope of this paper.

The fact that we encounter minima in curves T and D confirms the experience from simulations and experiments that the dynamics and the bifurcation diagram of the injected laser become more complicated as the linewidth enhancement factor α is increased [28]. Indeed, when α is increased past these minima extra organizing centers, T-points or double homoclinic bifurcation points, are born. These events are associated with infinitely many transitions = through saddles and extrema in surfaces of global bifurcations. Furthermore, general theory shows that the emerging T-points or double

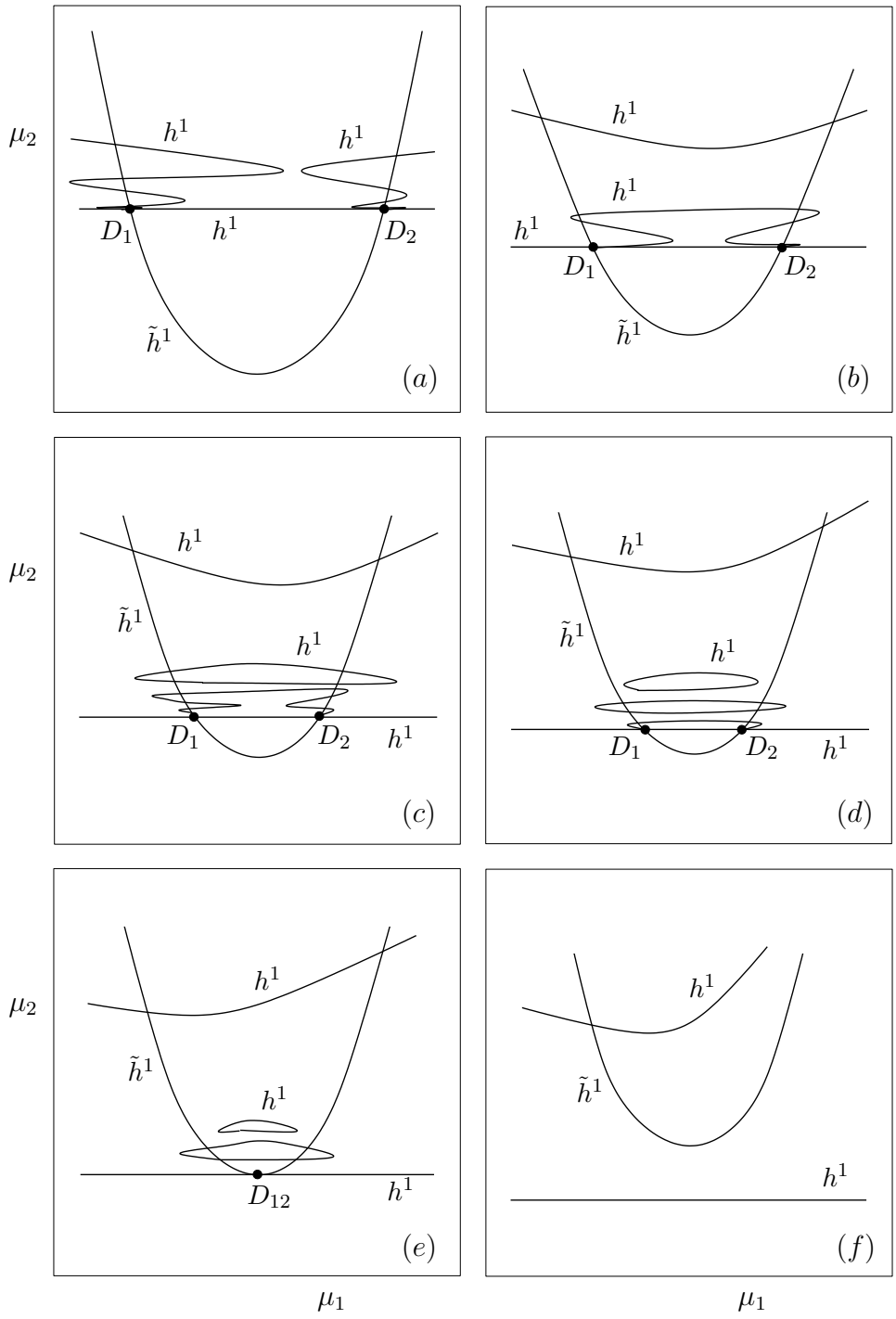

Figure 18. Sketch of how D_1 and D_2 come together and disappear when the section (paramaterized my μ_1 and μ_2) passes through a fold of the associated curve D of double-homoclinic orbits (compare with figure 17).

homoclinic bifurcation points are organizing centers that give rise to n-homoclinic orbits for any n.

As a final example of the increase in the complexity with α we show in figure 19 the

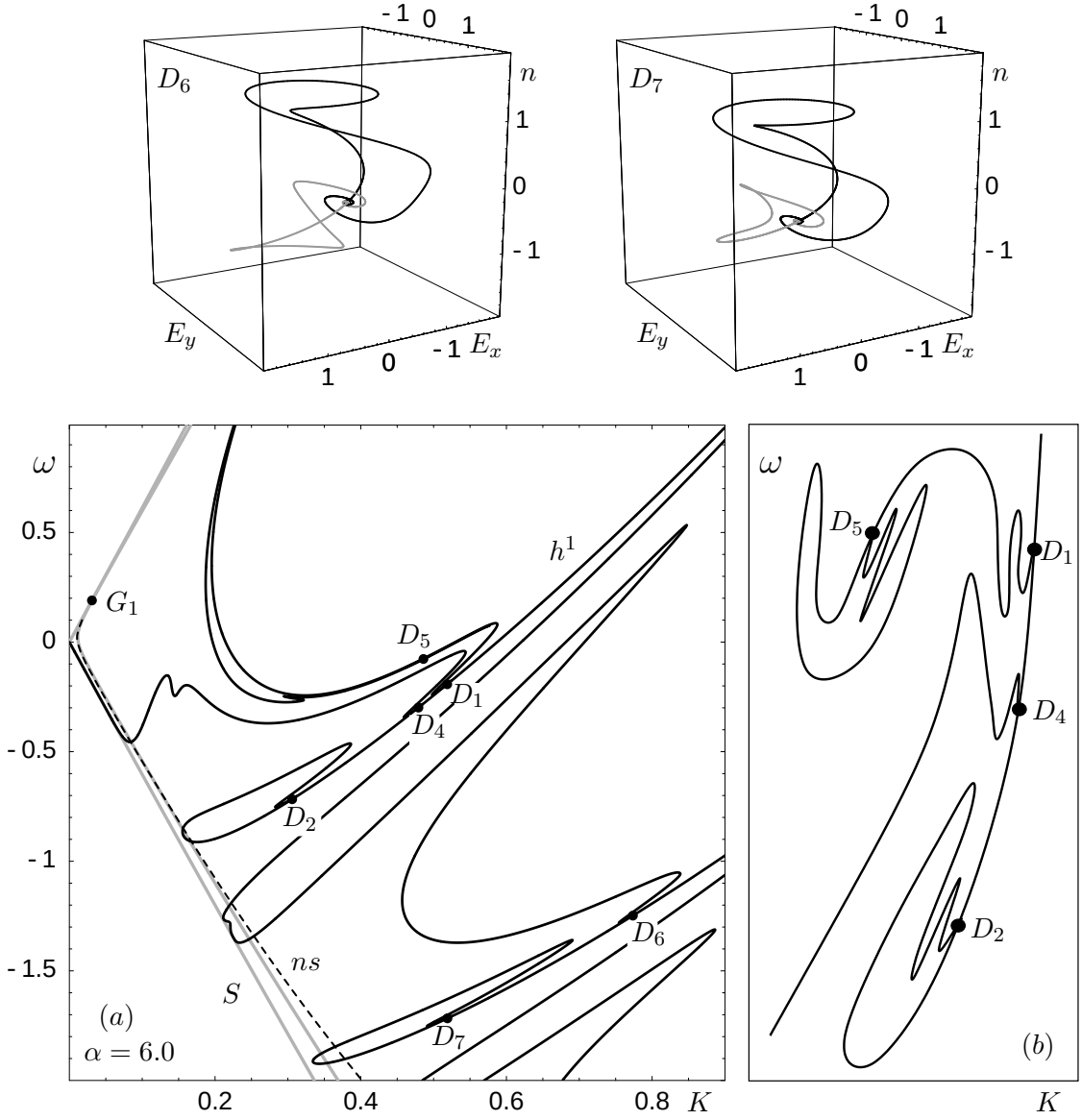

Figure 19. The (K, ω)-plane for $\alpha = 6.0$ near the point G_1 (compare with figure 2) and the phase portraits at the codimension-two points D_6 and D_7.

bifurcation diagram in the (K, ω)-plane for $\alpha = 6.0$ near the point G_1. Notice that we only show the different parts of the curve h^1 of one-homoclinic orbits, which form what is left from the left most homoclinic tooth near G_1; compare with figure 2(f). Near the points D_1 and D_2, that were already found for $\alpha = 4.5$, we find two new points D_4 and D_5; compare with figure 7. The different bifurcation curves are very close together, and the inset shows a topological sketch of the bifurcation diagram. Notice further that two extra double-homoclinic bifurcation points D_6 and D_7 have just been created. This is another example of the passage through a minimum of a curve D of double-homoclinic orbits; compare with figure 8.

Figure 19 shows that in the injected laser we are dealing with a type of cascade

phenomenon: complicated bifurcation scenarios found for one tooth also occur for all the other teeth when α is increased.

7. Conclusions

We presented a detailed study of the bifurcations of n-homoclinic orbits in the rate equations describing a semiconductor laser with optical injection. The corresponding curves of n-homoclinic bifurcations are organized in what we call homoclinic teeth — experimentally accessible regions inside the locking region of the laser. The analysis of the bifurcation diagram from a global viewpoint provided new insight into the nature of global bifurcations and allowed to identify a cascade phenomenon where complicated bifurcation scenarios repeat for subsequent homoclinic teeth.

The injection laser rate equations emerged as a concrete vector field in which complicated global bifurcations can be found and studied. Specifically, we found in this three-dimensional vector field (without any additional symmetries) T-point bifurcations and double-homoclinic orbits. By making extensive use of continuation techniques for homoclinic and heteroclinic orbits, it is possible to study these codimension-two global bifurcations themselves, and also to find out how they organize the corresponding bifurcation diagrams.

When changing a third parameter, we found a new phenomenon, namely complicated transitions in two-parameter bifurcation diagrams that are due to folds (in this case, minima) in codimension-two curves of global bifurcations. These 'codimension-two-plus-one events' come with accumulations of singularity transitions through saddles and extrema, which can be explained by the geometry of surfaces of global bifurcations in a three-dimensional parameters space.

Our results raise a number of questions of bifurcation theory. Especially the detailed study of the unfoldings of the 'codimension-two-plus-one events' remains a challenging task.

From the physical point of view, we presented here how the regions in which one may find multi-pulse excitability depend on the linewidth-enhancement factor α. Our results confirm that the larger the linewidth enhancement fact α, the more complex are the dynamics and bifurcations of an injected laser. Furthermore, we showed that multi-pulse excitability can be found in lasers with $\alpha = 1.0$ and even slightly below. In light of the good agreement between theory and experiment of the injection laser [60, 61, 62], this information may prove to be useful to experimentalists. Nevertheless, an experimental verification of multi-pulse excitability is quite difficult and remains an open challenge.

Acknowledgements

We thank Ale Jan Homburg for helpful discussions on the literature on codimension-two homoclinic bifurcations. The research of SW was funded by the US Department

of Energy under contract DE–AC04–94AL8500, and by Vrije Universiteit Amsterdam. The research of BK was supported by an Advanced Research Fellowship grant from the Engineering and Physical Sciences research Council (EPSRC).

References

[1] Shilnikov L P 1965 A case of the existence of a countable number of periodic orbits *Soviet Math. Dokl.* **6** 163–166.
[2] Shilnikov L P 1970 A contribution to the problem of the structure of an extended neighborhood of a rough state to a saddle-focus type *Math. USSR-Sb.* **10** 91–102.
[3] Guckenheimer J and Holmes P 1986 *Nonlinear Oscillations Dynamical Systems and Bifurcations of Vector Fields* Second Printing (New York:Springer).
[4] Kuznetsov Yu A 1995 *Elements of Applied Bifurcation Theory* Applied Mathematical Sciences **112** (New York:Springer).
[5] Arneodo A Argoul F Elezgaray J and Richetti P 1993 Homoclinic chaos in a chemical system *Physica D* **62** 134–169.
[6] Koper M 1995 Bifurcations of mixed-mode oscillations in a three-variable autonomous Van der Pol-Duffing model with a cross shaped phase diagram *Physica D* **80** 72–94.
[7] Sneyd J LeBeau A and Yule D 2000 Traveling waves of calcium in pancreatic acinar cells: model construction and bifurcation analysis *Physica D* **145** 158–179.
[8] Shil'nikov A Nicolis G and Nicolis C 1995 Bifurcation and predictability analysis of a low-order atmospheric circulation model *Int. Jour. Bif. and Chaos* **6** 1701–1711.
[9] Wieczorek S Krauskopf B and Lenstra D 2002 Multipulse Excitability in a Semiconductor Laser with Optical Injection *Phys. Rev. Lett.* **88** (6) 063901.
[10] Zimmermann M G, Firle S, Natiello M A, Hildebrand M, Eiswirth M, Bar M, Bangia A K, and Kevrekidis I G 1997 Pulse bifurcation and transition to spatiotemporal chaos in an excitable reaction-diffusion model. *Physica D* **110** 92–104.
[11] Glendinning P and Sparrow C 1986 T-points: A codimension two heteroclinic bifurcation *J. Statist. Phys.* **43** 479–488.
[12] Forysiak W Moloney J V and Harrison R G 1991 Bifurcations of an optically pumped three-level laser model *Physica D* **53** 162–186.
[13] Fernández-Sánchez F Freire E and Rodriguez-Luis A 2002 T-points in a $\mathbb{Z}_2$-symmetric electronic oscillator: (I) analysis *Nonlinear Dynamics* **28** 53-69.
[14] Green K Krauskopf B and Samaey G 2003 A two-parameter study of the locking region of a semiconductor laser subject to phase-conjugate feedback *SIAM J. of Appl. Dyn. Sys.* **2** 254–276.
[15] Algaba A Merino M Fernández-Sánchez F and Rodriguez-Luis A = 2002 Closed curves of global bifurcations in Chua's equation: a mechanism for their formation *Int. J. Bifur. Chaos* **13** (3) 609–616.
[16] Krauskopf B and Sieber J 2004 Bifurcation analysis of an inverted pendulum with delayed feedback control near a triple-zero eigenvalue singularity *Nonlinearity* **17** (1) 85–103.
[17] Bykov V V 2000 Orbit structure in a neighborhood of a separatrix cycle containing two saddle foci in Methods of qualitative theory if differential equations and related topics *American Math. Soc. Transl. Ser 2* **200** 87-97.
[18] Bykov V V 1993 The bifurcations of separatrix contours and chaos *Physica D* **62** 290–299.
[19] Homburg A J 2002 Periodic attractors strange attractors and hyperbolic dynamics near homoclinic orbits to saddle-focus equilibria *Nonlinearity* **15** 1029–1050.
[20] Shashkov M V and Turaev D V 1996 On the complex bifurcation set for a system with simple dynamics *Internat. J. Bif. Chaos* **6** (5) 949–968.
[21] Ovsyannikov I M and Shilnikov L P 1987 Systems with a saddle-focus homoclinic curve *Math. USSR-Sb.* **58** (2) 557–574.

[22] Champneys A R and Kuznetsov Yu A 1994 Numerical detection and continuation of codimension-two homoclinic bifurcations *Int. J.Bifur. Chaos* **4** (4) 785–822.
[23] Champneys A R Kuznetsov Yu A and Sandstede B 1996 A numerical toolbox for homoclinic bifurcation analysis *Int. J.Bifur. Chaos* **6** 867–887.
[24] Doedel E Champneys A Fairgrieve T Kuznetsov Yu Sandstede B and Wang X AUTO 97: Continuation and bifurcation software for ordinary = differential equations *http://indy.cs.concordia.ca/auto/main.html*
[25] Back A Guckenheimer J Myers M R Wicklin F J and Worfolk P A 1992 DsTool: Computer assisted exploration of dynamical systems *Notices Amer. Math. Soc.* **39** 303-309.
[26] van Tartwijk G H M and Lenstra D 1995 Semiconductor lasers with optical injection and feedback *Quant. Semiclass. Opt.* **7** 87–143.
[27] van Tartwijk G H M and Agrawal G P 1998 Laser instabilities: a modern perspective *Progr. Quant. Electron.* **22** 43–122.
[28] Wieczorek S Krauskopf B and Lenstra D 1999 A unifying view of bifurcations in a semiconductor laser subject to optical injection *Opt. Comm.* **172** (1-6) 279-295.
[29] Kobayashi S and Kimura T 1980 Injection locking characteristics of an ALGaAs semiconductor laser *IEEE J. Quantum Electron.* **16** 915–917.
[30] Lang R 1982 Injection locking properties of a semiconductor laser *IEEE J. Quantum Electron.* **18** (6) 976–983.
[31] Mogensen F Olesen H and Jacobsen G 1985 FM noise suppression and linewidth reduction in an injection-locked semiconductor laser *Electron. Lett.* **21** 696–697.
[32] Lugiato L A Narducci L M Bandy D K and Pennise C A = 1983 Breathing spiking and chaos in a laser with injected signal *Opt. Comm.* **46** 64–68.
[33] Lee E K Pang H S Park J D and Lee H 1993 Bistability and chaos in an injection-locked semiconductor laser *Phys. Rev. A* **47** (1) 736–739.
[34] Annovazzi-Lodi V Donati S and Manna M 1994 Chaos and locking in a semiconductor laser due to external injection *IEEE J. Quantum Electron.* **30** (7) 1537–1541.
[35] Kovanis V Gavrielides A Simpson T B and Liu J M 1995 Instabilities and chaos in optically injected semiconductor lasers *Appl. Phys. Lett.* **67** (19) 2780–2782.
[36] Erneux T Kovanis V Gavrielides A and Alsing P M 1996 Mechanism for period-doubling bifurcation in a semiconductor laser subject to optical injection *Phys. Rev. A* **53** (6) 4372–4380.
[37] Gavrielides A Kovanis V Varangis P M Erneux T and Lythe G 1997 Coexisting periodic attractors in injection-locked diode lasers *Quant. Semiclass. Opt.* **9** (5) 785–796.
[38] Spencer M B Lamb W E Jr. 1972 Laser with a transmitting window *Phys. Rev. A* **5** 884–892.
[39] Hwang S K and Liu J M 2000 Dynamical Characteristics of an optically injected semiconductor laser *Opt. Comm.* **183** 195–205.
[40] Chlouverakis K E and Adams M 2003 Stability maps of injection-locked laser diodes using the largest = Liapunov exponent *Opt. Comm.* **216** 405–412.
[41] Erneux T Gavrielides A and Kovanis V 1997 Low pump stability of an optically injected diode laser *Quant. Semiclass. Opt.* **9** (5) 811–818.
[42] Kovanis V Erneux T and Gavrielides A 1999 Largely detuned injection-locked semiconductor lasers *Opt. Comm.* **159** 177–183.
[43] Nizette M Erneux T Gavrielides A and Kovanis V 1999 Injection locked semiconductor laser dynamics from large to small detunings *Proc. SPIE* **3625** 679–689
[44] Nizette M Erneux T Gavrielides A and Kovanis V 2002 Averaged equations for injection locked semiconductor lasers *Physica D* **161** 220–236.
[45] Solari H G Oppo G L 1994 Laser with injected signal: perturbation of an invariant circle *Opt. Comm.* **111** 173–190.
[46] Zimmermann M G Natiello M A and Solari H 1997 Shilnikov-Saddle-node interaction near a codimension 2 bifurcation: laser with injected signal *Physica D* **109** (3-4) 293–314.
[47] de Jagher P C van der Graaf W A and Lenstra D 1996 Relaxation-oscillation phenomena in an

injection locked semiconductor laser *Quant. Semiclass. Opt.* **8** 805–822.
[48] Krauskopf B van der Graaf W A and Lenstra D 1997 Bifurcations of relaxation oscillations in an optically injected diode laser *Quant. Semiclass. Opt.* **9** 797–809.
[49] Krauskopf B Tollenaar N and Lenstra D 1998 Tori and their bifurcations in an optically injected semiconductor laser *Opt. Comm.* **156** 158–169.
[50] Solari H G, Eschenazi E, Gilmore R, and Tredicce J R, Influence of coexisting attractors on the dynamics of a laser system, *Opt. Comm.* **64** 49–53.
[51] Wieczorek S Krauskopf B and Lenstra D 2000 Mechanisms for multistability in a semiconductor laser with optical injection *Opt. Comm.* **183** (1-4) 215–226.
[52] Krauskopf B Wieczorek S and Lenstra D 2000 Different types of chaos in an optically injected semiconductor laser *Appl. Phys. Lett.* **77** (11) 1611–1613.
[53] Wieczorek S Krauskopf B and Lenstra D 2001 Sudden chaotic transitions in an optically injected semiconductor laser *Opt. Lett.* **26** (11) 816-818.
[54] Wieczorek S Krauskopf B and Lenstra D 2001 Unnested islands of period-doublings in an injected semiconductor laser *Phys. Rev. E* **64** 056204 1-9.
[55] Yeung M K S and Strogatz S H 1998 Nonlinear dynamics of a solid-state laser with injection *Phys. Rev. E* **58** (4) 4421–4435; Erratum 2000 *Phys. Rev. E* **61** (2) 2154.
[56] Mayol C Natiello M A and Zimmermann M G 2001 Resonance structure in a weakly detuned laser with injected signal *Int. J. Bif. Chaos* **11** 2587–2605.
[57] Zimmermann M G Natiello A and Solari H 2001 Global bifurcations in a laser with injected signal: beyond Adler's approximation *CHAOS* **11** 500–513.
[58] Krauskopf B and Wieczorek S 2002 Accumulating regions of winding periodic orbits in optically driven lasers *Physica D* **173** (1-2) 97–113.
[59] Krauskopf B Schneider K R Sieber J Wieczorek S Wolfrum M 2003 Excitability and self-pulsations near homoclinic bifurcations in semiconductor laser systems *Opt. Commun.* **215** 367–379.
[60] Wieczorek S Simpson T B Krauskopf B and Lenstra D = 2002 Global quantitative predictions of complex laser dynamics *Phys. Rev. E* **65** (4) 045207R.
[61] Wieczorek S Simpson T B Krauskopf B and Lenstra D = 2003 Bifurcation transitions in an optically injected diode laser: theory and experiment *Opt. Commun.* **215** 125–134.
[62] Simpson T B 2003 Mapping the nonlinear dynamics of a DFB semiconductor laser subject to external optical injection *Opt. Commun.* **215** 135–151.
[63] Simpson T B Liu J M Huang K F and Tai K 1997 Nonlinear dynamics induced by external optical injection in semiconductor lasers *Quant. Semiclass. Opt.* **9** (5) 765–784.
[64] Eriksson S and Lindberg A M 2001 Periodic oscillations within the chaotic region in a semiconductor laser subject to optical injection *Opt. Lett.* **26** (3) 142–144.
[65] Chow S-N and Lin X-B 1990 Bifurcation of a homoclinic orbit with a saddle-node equilibrium *Differential Integral Equations* **3** 435–466.
[66] Deng Bo 1990 Homoclinic bifurcations with nonhyperbolic equilibria *SIAM J. Math. Anal.* **21** 693–720.
[67] Bai F and Champneys A R 1996 Numerical computation of saddle-node homoclinic orbits of co-dimension = one and two J. Dyn. Stab. Syst. **11** 325–346.
[68] Schecter S 1993 Numerical computation of saddle-node homoclinic bifurcation points *SIAM J. Numer. Anal.* **30** 1155–1178.
[69] Belyakov L 1984 Bifurcation of systems with homoclinic curve of a saddle-focus with = saddle quantity zero *Mat. Zam.* **36** 681–689.
[70] Gonchenko S V Turaev D V Gaspard P and Nicolis G = 1997 Complexity in the bifurcation structure of homoclinic loops to a saddle-focus *Nonlinearity* **10** 409–423.
[71] Wieczorek S and Lenstra D 2004 Spontaneously excited pulses in an optically driven laser submitted to *Phys. Rev. E* **69** 016218.
[72] Golubitsky M and Schaeffer D G 1985 *Singularities and Groups in Bifurcation Theory, Vol. 1* Applied Mathematical Sciences **51** (New York:Springer).